A Multi-Agency Experiment on Internal Wave Energy, Mixing, and Interactions and their Representation in Global Ocean Models and Operational Forecasts

Maarten C. Buijsman,[a] Amy F. Waterhouse,[b] Edward D. Zaron,[c] Badarvada Yadidya,[d] Chengzhu Xu,[c] Victoria Whitley,[e] Jacob O. Wenegrat,[e] Jinbo Wang,[f] Alan J. Wallcraft,[g] Dheeraj Varma,[a] Babette C. Tchonang,[xx] Oladeji Siyanbola,[a] Jay F. Shriver,[h] Vitalii A. Sheremet,[i] Uwe Send,[b] Keshav J. Raja,[g] Kurt Polzin,[i] Hans E. Ngodock,[h] Aurelie J. Moulin,[j] Grant Meiners,[b] Andrew J. Lucas,[b,k] Matthias Lankhorst,[b] Joseph J. Kuehl,[l] Samuel M. Kelly,[m] Yonglin Huang,[y] Caeli Griffin,[b] James B. Girton,[j] J. Thomas Farrar,[i] Zihan Chen,[e] Eric P. Chassignet,[g] Matthew J. Carrier,[h] Annalisa Bracco[n] Brian K. Arbic,[d] Magdalena Andres,[i] Mujeeb A. Abdulfatai,[a]

[a] *University of Southern Mississippi*

[b] *Scripps Institution of Oceanography*

[c] *Oregon State University*

[d] *University of Michigan*

[e] *University of Maryland, College Park*

[f] *Texas A & M University*

[g] *Florida State University*

[xx] *NASA Jet Propulsion Laboratory*

[h] *U.S. Naval Research Laboratory*

[i] *Woods Hole Oceanographic Institution*

[j] *University of Washington Applied Physics Laboratory*

[k] *Dept. of Mechanical and Aerospace Engineering, U.C. San Diego*

[l] *University of Delaware*

[m] *University of Minnesota Duluth*

[n] *Georgia Institute of Technology & CMCC*

Corresponding author: Maarten C. Buijsman, maarten.buijsman@usm.edu

ABSTRACT: As part of a National Oceanographic Partnership Program (NOPP) project, seven teams—comprised of investigators from universities, federal laboratories, and industry—are collaboratively investigating the generation, propagation, and dissipation of internal waves in the global ocean using complementary, state-of-the-art observations and model simulations. Internal waves, generated by the interaction of tides, winds, and mean flows, permeate the ocean and influence its physical and biogeochemical state. Internal waves transport scalar and vector properties—both geographically and across scales—and contribute to irreversible mixing, they modulate acoustic propagation, and they complicate the identification of sub-inertial (e.g., geostrophic) flows in observations. For these reasons, accurately representing internal waves in global ocean forecast models is a high priority. The collaborations reported here are improving the understanding of the internal wave life cycle and enhancing model skill in simulating it. Three observational teams are collecting *in situ* data using (1) re-deployable moored arrays that resolve internal waves from multiple directions, (2) global deployments of profiling floats that measure internal wave energy fluxes, shear, and mixing, and (3) high-resolution arrays that focus on bottom boundary layer processes. Four modeling teams are guiding the design and placement of these observation platforms and using the collected observations to (1) improve internal wave representation and dissipation in ocean models, (2) conduct high-resolution process studies, and (3) implement data assimilation in idealized, regional, and global simulations. These efforts are further supported by high-resolution sea-surface height measurements from the new SWOT satellite, which provide context for in-situ observations and improve ocean forecasting systems.

SIGNIFICANCE STATEMENT: A collaboration among scientists from U.S. universities, national laboratories, and industry is advancing our understanding and prediction of internal waves in the global ocean. These waves—characterized by vertical scales of tens to hundreds of meters and horizontal scales of tens to hundreds of kilometers—play a critical role in maritime commerce, naval operations, and ocean circulation. The team integrates novel observational approaches, including internal wave resolving moored arrays, ship-of-opportunity float deployments, bottom boundary layer distributed sensor networks, and satellite wide-swath altimetry, with cutting-edge global, regional, and process-model simulations. Together, these efforts are improving the representation of internal wave processes in ocean models and enhancing their predictive capabilities for operational forecasts.

CAPSULE: Combining novel measurement and modeling approaches to study the life cycle of internal waves in the global ocean

1. Introduction

Analogous to surface gravity waves that occur at the interface between air and water, internal gravity waves exist at the interface between lighter and denser water layers in the ocean interior. Unlike surface gravity waves, which have amplitudes of meters, wavelengths of tens of meters, and periods of seconds, the largest internal waves have amplitudes of 100 m or more, wavelengths of hundreds of kilometers, and periods of hours (e.g., Gill 1982). Since the first recorded measurements of internal waves in 1893 (Nansen 1897), their life cycle has been a topic of active research because internal waves provide a fundamental conduit by which energy is input into the global ocean. This can occur either via direct forcing by winds or tides, or indirectly through exchange with subinertial flows. Energy eventually cascades to smaller scales, where internal wave breaking is the rate-limiting step for the turbulent mixing that plays a role in sustaining the meridional overturning circulation (Munk and Wunsch 1998a; MacKinnon et al. 2017; Melet et al. 2016; Buijsman et al. 2019). More broadly, internal waves are fundamental partners with sub-inertial flows in closing oceanic mass, momentum, energy, and potential vorticity budgets.

Though internal waves' expression on the sea surface is subtle, they strongly influence many aspects of ocean processes, and maritime commerce and operations. Wind- and tidally-generated internal waves, known as near-inertial waves and internal tides, respectively, can travel 1000s of

km across ocean basins (Fig. 1; Zhao et al. 2016; Buijsman et al. 2025; Raja et al. 2022) increasing internal wave energy levels and mixing along the continental margins (Kelly et al. 2013; Siyanbola et al. 2023, 2024), with detection even in the surf zone (Kumar et al. 2021). As they cascade to smaller scales, breaking internal waves drive diapycnal mixing that disperses heat, nutrients and sediments (e.g., Lucas et al. 2011; Villamaña et al. 2017; Boegman and Stastna 2019; Zulberti et al. 2020).

Because energetic internal waves impact the transmission of acoustic signals (e.g., Little 1966; Headrick et al. 2000; Lynch et al. 2010; Colosi 2016; Hiron et al. 2025) and underwater vessel navigation (e.g., Little 1966; Neuman 2021; Chen et al. 2022), it is important to predict their occurrence, energy, and phase, for example, with hydrodynamic and/or altimetry-constrained models (Zaron 2019a; Yadidya et al. 2024).

Two thematic lines of research on internal waves have emerged that suggest a surface wave analogy, in which the wave field is recognized as being comprised of two parts. The first, the wind wave field, relates to the local wind. The wind wave analogy for internal waves is generally quantified with spectral representations introduced in Garrett and Munk (1975). The second analogy is with swell, which is quasi-deterministic and possibly related to distant storms (Munk and Wunsch 1998b). Internal swell (Alford 2003) are those waves with the largest group velocities, limited to the lowest vertical modes, that minimally interact with other waves and sub-inertial flows.

Early modern day[1] research on internal waves was largely guided by the wind wave field framework and thus developed observational tools that were good at shorter space and time scales and a theoretical focus on explaining the possibility of a 'universal' spectrum (Briscoe 1975; Wunsch and Ferrari 2004; Garrett and Munk 1979; Munk 1981; Müller et al. 1986). This line of investigation provided a direct link to mixing, but not to the regional variability set up by the patterns of larger scale forcing. In the post-1993 satellite altimetry era, regional patterns of the internal wave field could be identified from observations of ocean surface height as long-wavelength internal waves at tidal frequencies (Ray and Mitchum 1996; Carrère et al. 2021). Altimetry also provided the first reliable estimate for the generation rate of internal waves by tides at large-scale topographic features in the deep ocean (Egbert and Ray 2000), thus making a quantitative link to the mechanical energy

[1] Polzin and McDougall (2022) locate the dawn of modern oceanography with the development of near-continuously profiling instrumentation in the early 1970s

budget of the global ocean. Additional insights into the spatio-temporal global internal field were obtained when tidal forcing (e.g., Niwa and Hibiya 2001; Simmons et al. 2004) and both tidal and high-frequency wind forcing (e.g., Arbic et al. 2010; Waterhouse et al. 2014) were incorporated into global circulation models. Moreover, Polzin and Lvov (2011) suggested that if one averages the energy spectra over multiple eddy time scales, regional variability in the spectral fits underpinning the wind wave analogy exists and, possibly, can be understood in terms of the regional variability in the major sources, tides and eddies, and the major nonlinear transfer mechanisms. We are now at the point that regional numerical simulations (e.g., Nelson et al. 2020; Siyanbola et al. 2023; Skitka et al. 2024a,b), taking boundary conditions from global numerical simulations, can provide diagnostics about those hypothetical linkages between internal 'swell' and internal 'wind' waves that can justify regional patterns of mixing as observed in Whalen et al. (2015).

Parallel to recent advances in our theoretical understanding and observational characterization of internal wave dynamics, the development of global ocean models incorporating realistic tidal and atmospheric forcing has significantly enhanced our capacity to investigate ocean internal waves, particularly their spatio-temporal variability (Arbic 2022). Several developments have contributed to this. Foremost, the continued increase in computational power has facilitated the increase of grid resolutions that resolve smaller-scale internal waves. The accuracy of surface tides, and thus tidally generated internal waves (internal tides) has improved with the inclusion of a spatially varying self attraction and loading (SAL) term in conjunction with a Kalman filter (Ngodock et al. 2016) and linear wave drag formulations that dampen the surface and internal tides (e.g., Arbic et al. 2004; Buijsman et al. 2015; Xu and Zaron 2025). The accuracy of the internal tides, in phase and amplitude, has also improved due to data assimilation (DA), which ensures the background flow is simulated more realistically (e.g., Luecke et al. 2017; Yadidya et al. 2024). Finally, the improvement of the fidelity of wind-generated near-inertial waves in global ocean simulations is attributed to increases in model resolution and wind forcing frequency, the type of wind product used, and two-way atmosphere-ocean coupling (e.g., Furuichi et al. 2008; Simmons and Alford 2012; Flexas et al. 2019; Raja et al. 2022; Sun et al. 2024). Nonetheless, substantial challenges remain in improving model representations of internal waves, and energy dissipation pathways. Ongoing validation against high-resolution in situ and satellite observations is critical for constraining model uncertainties and guiding future developments.

We are a large team of academic, federal, and industry partners that is collaborating to substantially advance our knowledge on internal waves as part of a National Oceanographic Partnership Program (NOPP) Global Internal Waves (GIW) project "A Global Multi-Agency Experiment on Internal Wave Energy, Mixing and Interactions in the Ocean and their Representation in Global Ocean Models and Operational Forecasts". We have a diverse expertise in a broad range of tools and physical processes connected with internal waves, and we are motivated by improving the representation of internal waves in numerical models. Our team has been coordinating large observational field programs, designed to cover vast ranges of temporal and spatial scales across the global ocean basins (Fig. 1). By leveraging *in situ* instrumentation, remote sensing data and numerical models we aim to address the following research questions:

1. What are the primary processes by which internal waves dissipate, how do they vary across scales, and what are the implications for ocean mixing?

2. Do model simulations capture the internal wave life cycle with enough fidelity to provide realistic estimates of the propagation and arrival of both tidal and broadband internal wave energy?

3. How do the observed internal waves compare with the global model predictions in terms of intensity, variability and modal structure?

In this paper we highlight recent developments, enabled by this NOPP GIW, in observing and simulating internal waves and in internal wave theory. These developments are broadly categorized as follows: (1) understanding internal wave life-cycle processes including generation, propagation, and dissipation, (2) instrumentation and array design, and (3) model improvement and validation using observations. In the remainder of this paper, we present advances in internal wave observations and simulations in Section 2. We finish with a discussion on potential future developments in Section 3.

2. Methods and Results

a. Observational Techniques

The NOPP GIW observations serve a dual purpose: (1) understanding internal wave processes and (2) the validation of (global) ocean model simulations. In this section we discuss an In-

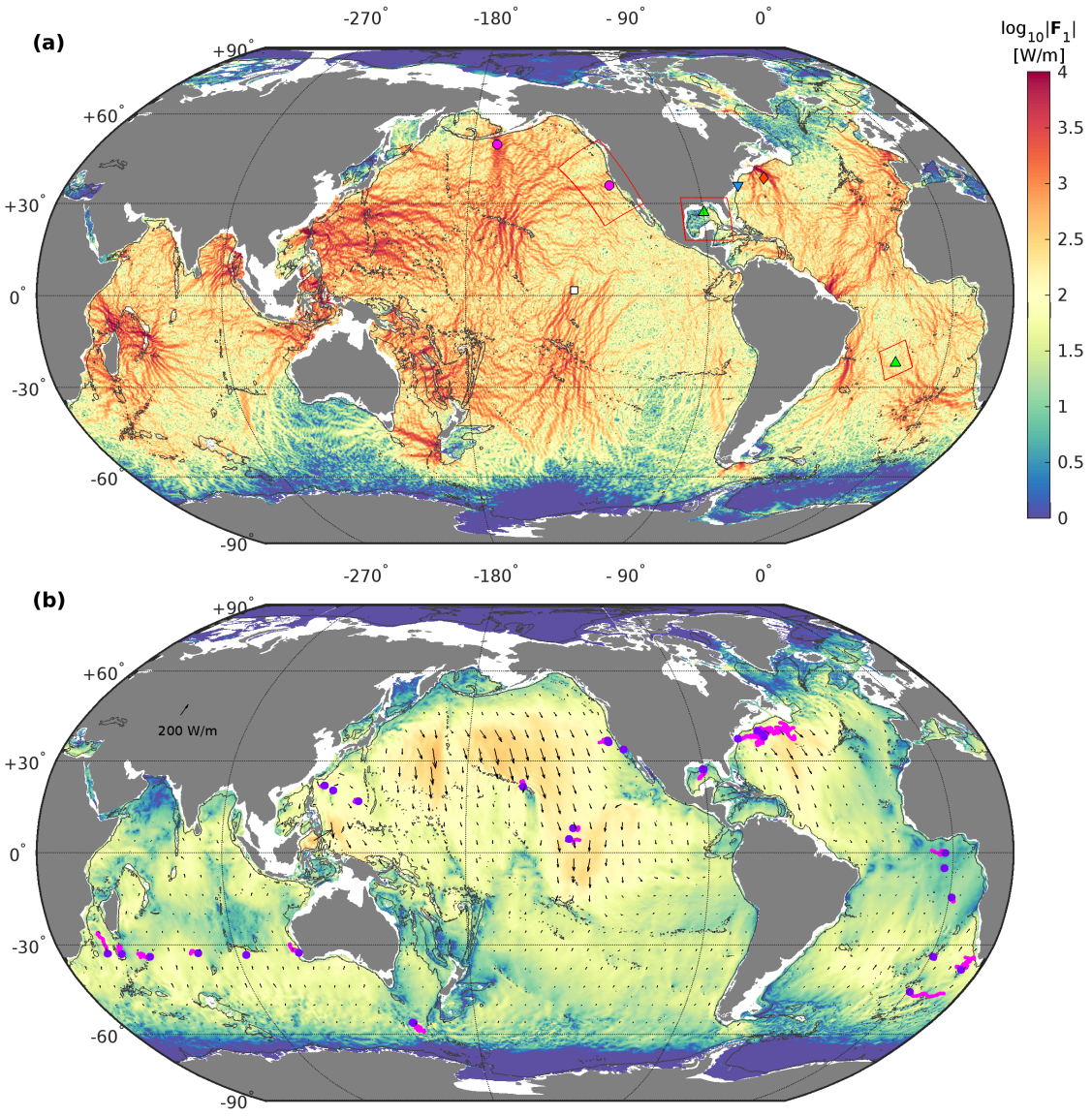

FIG. 1: The M_2 mode-1 internal tide energy flux radiates from ridges and shelves in (a), while the wind-generated near-inertial mode-1 energy flux is directed equatorward from the mid-latitudes in (b). Fields in (a) are extracted from a $1/25°$ Hybrid Coordinate Ocean Model (HYCOM; Bleck 2002) simulation (Buijsman et al. 2020) and time-averaged over the first two weeks of September 2016. Fields in (b) are extracted from an $1/12.5°$ HYCOM simulation (Buijsman et al. 2020) and time-averaged over a year from from October 2011 to September 2012. In (a) regional model simulation boundaries are marked as the red curves (Figs. 10, 12, and 13). The colored symbols represent the following NOPP GIW observations: IWR Arrays (magenta circles; Figs. 2 and 3), the Distributed Sensor Network (green triangles; Fig. 6) and EM-APEX float tracks (magenta dots in (b) with the deployment location shown with dark purple dot; Fig. 5). As part of NOPP GIW, CPIESs have been added to other project arrays: Mixing belOw Tropical Instability waVEs (MOTIVE; white square), Task Force Ocean New England Seamount Acoustics Experiment (TFO/NESMA; orange diamond), and the Mid-Atlantic Bight (MAB)-SWOT crossover (blue upside down triangle).

ternal Wave Resolving (IWR) Array, coincident Surface Water and Ocean Topography (SWOT) observations, velocity and turbulence profiling floats, and a distributed sensor network.

Internal Wave Resolving Array

An IWR Array was designed to detect multiple internal tide beams simultaneously. The array combines a central mooring to resolve the waves' modal structure surrounded by an antenna of vertically-integrated measures of the speed and direction of beam propagation. Before deployment, coordination with the NOPP GIW modeling teams (see Section b) allowed for the optimization of the central mooring and antenna (Fig. 2d-f).

This location was chosen for the NOPP GIW program because it features variable tidal internal wave energy fluxes generated remotely, e.g., from Hawai'i, and locally from the Mendocino Escarpment and shelf break (Figs. 1a and 2b). The IWR array (Fig. 2c) comprised eight current- and pressure-sensor equipped inverted echo sounders (CPIESs) in a 70-km diameter circle surrounding a densely instrumented, full-depth hybrid CTD-velocity-wirewalker-dynamic height mooring ("SIO hybrid mooring"). An additional PIES (i.e., a CPIES without the current sensor) was co-located with the central mooring. The IWR Array was first deployed off the coast of California at 35° 55.02' N, 125° 02.64' W, coinciding with the NASA/JPL SWOT Cal/Val (Wang et al. 2025).

The central hybrid mooring of the IWR Array measured the full-depth vertical structure of temperature, salinity and velocity for 20 months (Fig. 3) using a new design that was originally developed to obtain full-water column measurements for the NASA SWOT Cal/Val mission (Wang et al. 2022, 2025). It is a "hybrid" mooring due to the novel combination of an upper water column Wirewalker profiler (Pinkel et al. 2011) and a subsurface mooring section consisting of CTD sensors, multiple thermistors, current meters, and two long-range (75 kHz) acoustic Doppler current profilers (ADCPs; Tchonang and coauthors 2025; Fig. 2a). On average, a vertical profile of the upper 500 m with 1 m vertical resolution was collected every 30 min by the Wirewalker–or more than 25,000 500 m profiles over the length of the IWR deployment. The combination of velocity and density observations allowed the behavior of the full-ocean-depth internal wave field to be quantitatively examined across frequencies spanning the inertial frequency (f) to the buoyancy frequency (N) (Fig. 3b, h-j). This 'top-to-bottom, f to N' characterization of the internal wave field for more than 600 days is a first for an open ocean mooring. During this deployment, the mooring telemetered real-time observations to a web-based server at SIO/UCSD (`mooring.ucsd.edu`). The adjacent central PIES was outfitted with an acoustic modem (modem-PIES) and also returned real-time data.

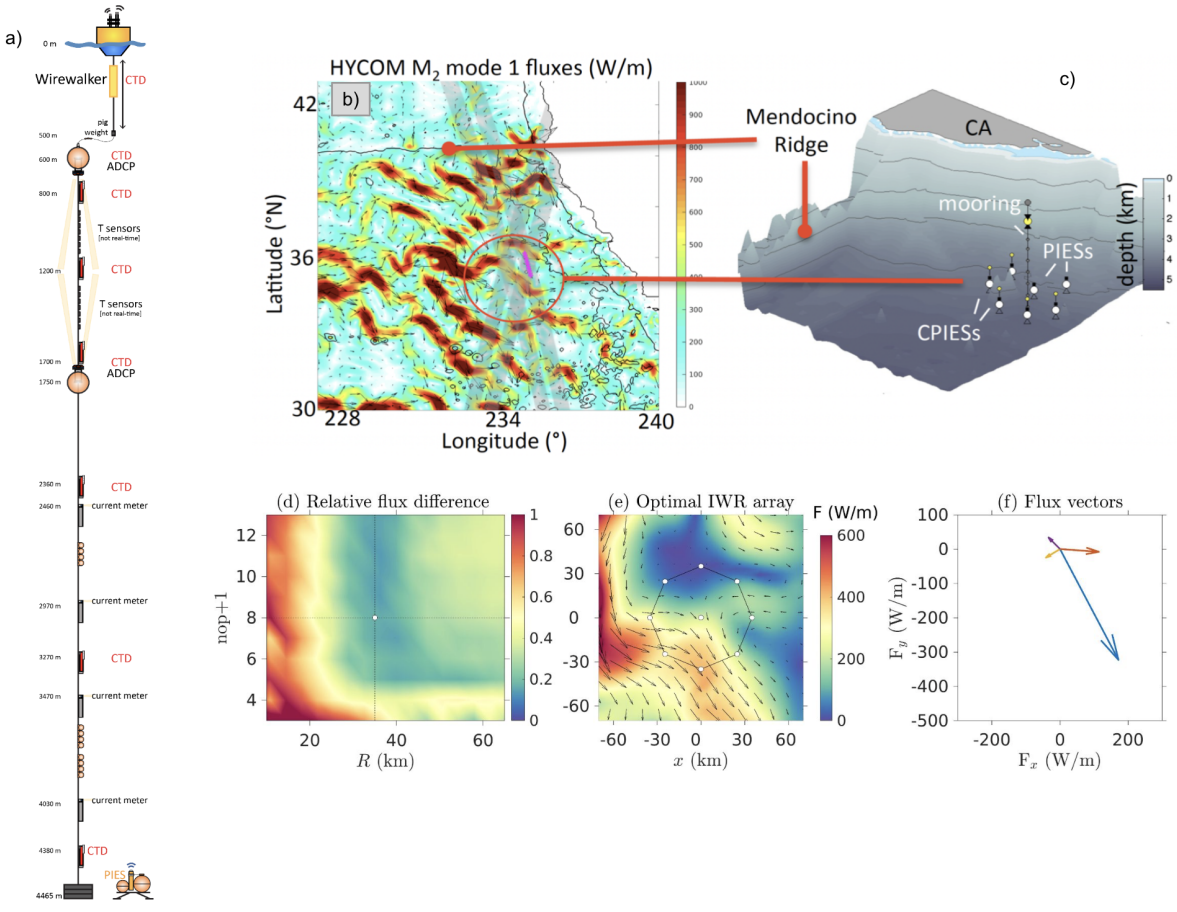

FIG. 2: Schematics for the first IWR Array deployment during the 2023 SWOT Calibration/Validation (Cal/Val) program. (a) SIO hybrid CTD-velocity-wirewalker-dynamic height mooring ("SIO hybrid mooring"; Wang et al. (2022)), consisting of a surface buoy, profiling Wirewalker in the upper 500 m (with a Nortek Signature 1000 kHz ADCP, RBR CTD, and real-time telemetry). A taut subsurface mooring (600 – 4500 m depth) was coupled to the surface buoy and Wirewalker via a catenary. The taut section of the mooring was instrumented with a series of current meters (Long Range 75 kHz ADCPs and Nortek Aquadopps), SBE37 CTDs, and RBR SoloTs. (b) As part of the pre-deployment planning, the modeled mode-1 semidiurnal (M_2) energy flux from a global $1/25°$ HYCOM simulation was used to guide the IWR Array placement. The NASA SWOT Cal/Val sites are marked with magenta crosses (Wang et al. 2025). (c) Schematic of the deployed IWR Array consisting of the SIO hybrid mooring surrounded by CPIESs (location of the continental slope is exaggerated). (d) Relative vector difference between the sum of M_2 mode-1 unidirectional energy fluxes derived from the Multi-VARiable Plane wave fit (MVARP) technique (Varma et al. 2025) and the undecomposed mode-1 fluxes from the HYCOM simulation, shown as a function of array radius (R) and the number of CPIESs (nop) of a circular IWR array. (e) Optimal configuration of the IWR array with $R = 35$ km and $nop = 8$, overlaid on the M_2 mode-1 flux of HYCOM. (f) First four dominant mode-1 internal wave flux vectors obtained with MVARP.

The spacing of the CPIESs distributed in a circle around the central site was chosen based on the capability of the IWR array to resolve waves from multiple directions (Fig. 2d-f). The CPIESs measured round-trip surface-to-bottom acoustic travel time (τ), bottom pressure and temperature, and near-bottom currents at 50 m above the seabed.

Observations from the 20-month deployment illustrate the seasonal variability of stratification, particularly in the upper ocean (Fig. 3a). While the modeled stratification captures some of the observed variability, there are many high-frequency events that were not captured in the model (Fig. 3b). The high-resolution profiling (in both depth and time) of the Wirewalker in the upper 500 m of the central mooring provided a detailed view of temperature, salinity, velocity and shear (Fig. 3g-j). In this month-long snapshot, the hybrid mooring captured both the semidiurnal tidal variability along with an event-scale near-inertial wave event. The CPIESs detected τ anomalies associated with the internal tide's displacement of the isotherms (Fig. 3c and d, inset), superimposed on the region's mesoscale variability.

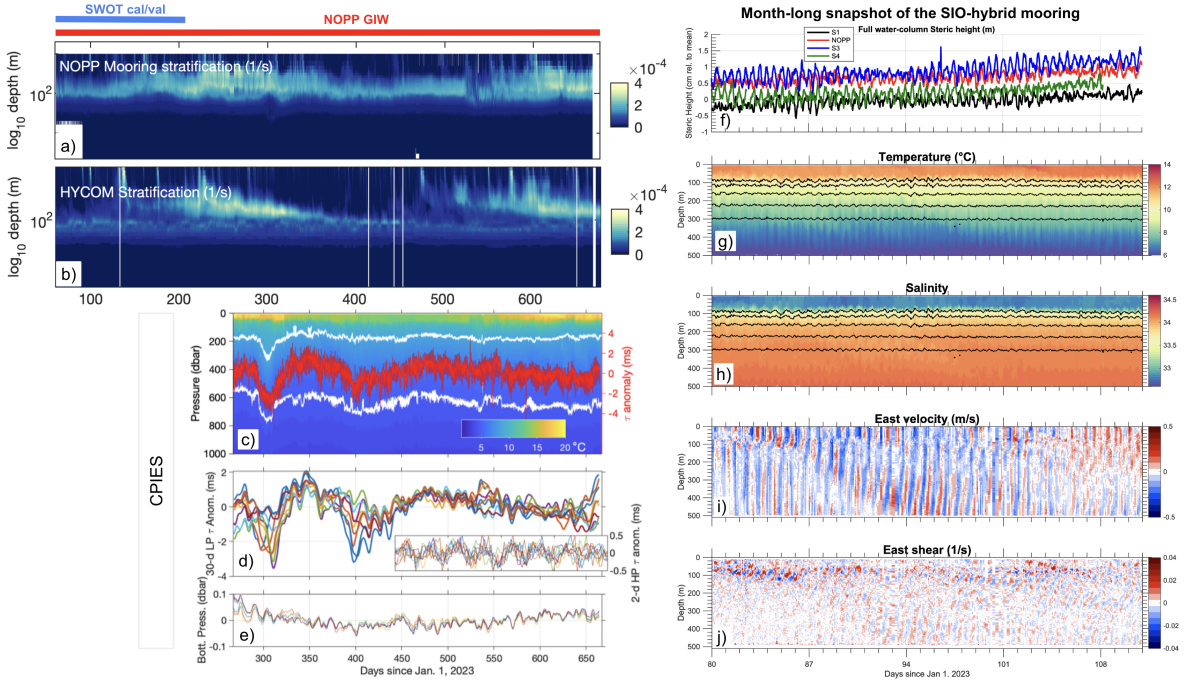

FIG. 3: Observations collected over the 20 month IWR Array deployment (SWOT 2024b), coordinated with the NASA SWOT Cal/Val program. The duration of each program is noted by the blue (SWOT Cal/Val) and red (NOPP GIW) overbars in (a). (a) Observed stratification, plotted in log(depth), shows the variability of the upper ocean stratification, much of which is captured by (b) the simulated stratification from a $1/25^\circ$ HYCOM simulation during the same time period. (c-e) Observations from the the 8 CPIESs (C1-C8) surrounding the SIO hybrid mooring and a modem-PIES (C9) located adjacent to the central mooring. (c) Hourly temperature profiles from the upper 1000 m (left y-axis, shading) with the 5 and 9°C isotherms highlighted in white and the hourly τ anomaly from C9 superimposed (right y-axis, red curve). Mesoscale variability results in isotherm displacements of up to 170 dbar that correspond to ~20 ms τ anomalies. (d) 30-day lowpass filtered τ anomalies at each site in the array, with the inset showing the 2-day highpass filtered τ anomalies over a 4-day period; the semidiurnal internal tide causes 1 ms τ anomalies that correspond to ~20 dbar isotherm displacements. (e) 15-day low pass filtered bottom pressure at each site; bottom pressure is remarkably coherent across the sites. Right panels show a month-long snapshot from the central mooring between yearday 80 - 111 (mid-March to Mid-April, 2023) including (f) the full-depth steric height from all 4 SIO hybrid moorings deployed as part of the NASA SWOT Cal/Val, including the central NOPP GIW mooring (red line). This mooring also includes high resolution measurements in the upper 500m of (g) temperature, (h) salinity, (i) zonal velocity (positive eastward), and (j) zonal shear highlighting the ability of the hybrid mooring to observe internal waves.

Surface Water and Ocean Topography Mission

While regional field campaigns provide detailed observations at single locations, studying internal waves and tides globally requires remote sensing (Ray and Mitchum 1996; Carrère et al. 2021). As propagating internal waves displace and deform the thermocline, they induce steric changes in the upper ocean, manifesting as variations in sea surface height (SSH). Over the past three decades, nadir altimeters have successfully mapped coherent, mode-1, long-wavelength internal tides phase-locked to tidal forcing. However, incoherent internal tides and smaller-scale nonlinear internal gravity waves remain unmapped due to spatial and temporal gaps in the nadir altimeter tracks. NASA's SWOT mission, launched on December 16, 2022, transforms global studies by resolving smaller wavelengths, including higher vertical modes, using its Ka-band interferometer (KaRIn) (Wang et al. 2025). KaRIn resolves km-scale SSH structures across a 120-km swath, enabling studies of small-scale linear and nonlinear internal waves, as shown in recent studies (e.g., Qiu et al. 2024; Archer et al. 2025). The SSHA gradient (Fig. 4) highlights small-scale, high-amplitude SSH signals from nonlinear internal tides and solitary waves. A $1/50^\circ$ HYCOM simulation resolves these solitary waves but not the full spectrum. Leveraging SWOT's rich observational information to enhance modeling remains an area of active research.

Velocity and Turbulence Profiling Floats (SQUID)

In order to permit characterization of a broad range of oceanic internal wave environments and facilitate the global validation of internal wave resolving models, we are deploying autonomous profiling floats (Fig. 5a) measuring temperature, salinity, horizontal currents, and turbulent mixing from cruises of opportunity. The floats (EM-APEX, or Electro-Magnetic Autonomous Profiling EXplorers; Sanford et al. 2005) are similar to those used in the global Argo array but with the addition of electrodes sensing the conducting seawater's motion (Fig. 5b) in the geomagnetic field (Sanford 1971), as well as fast-response FP07 thermistors to measure the rate of temperature gradient dissipation by turbulence (Fig. 5d; Lien et al. 2016). This component of NOPP GIW is denoted "SQUID" (Sampling QUantitative Internal-wave Distributions) and aims to span the broad range of internal wave environments and forcing and propagation parameters (e.g., wind, tide, mesoscale eddies, water depth, topographic roughness, stratification, and latitude).

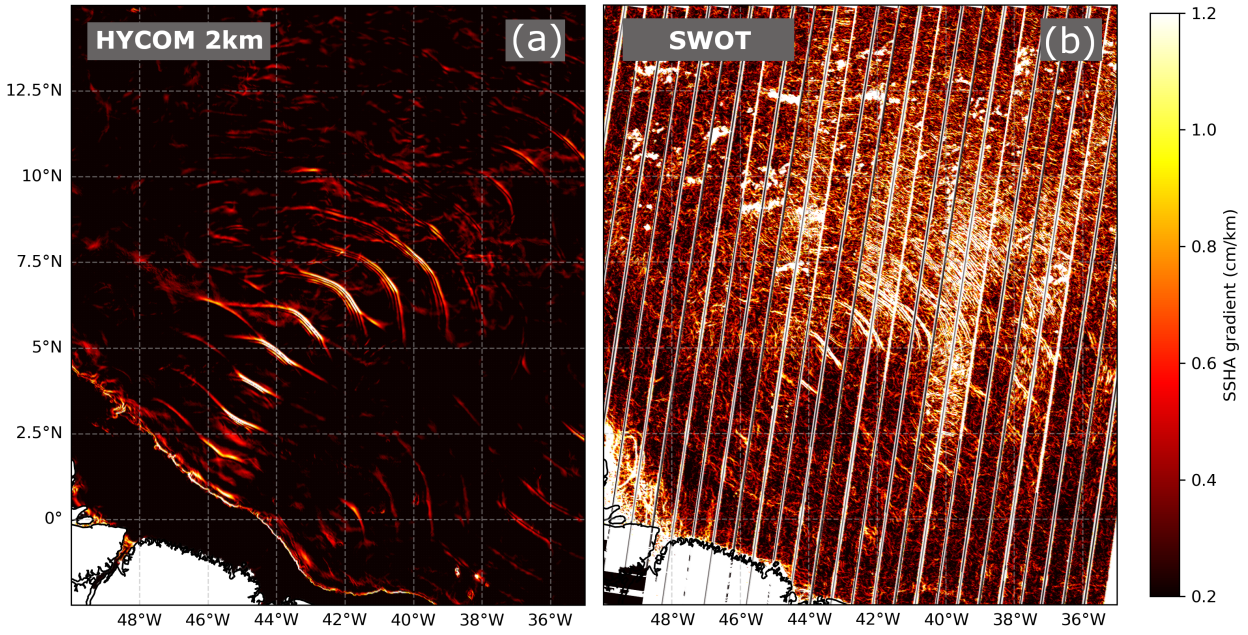

FIG. 4: Nonlinear internal tides are observed radiating from the Amazon shelf in sea surface height gradient maps based on (a) a 1/50° HYCOM simulation of the Atlantic Ocean (Xu et al. 2022) and (b) SWOT wide swath altimetry with a resolution of 2 km. SWOT data are taken during cycle 28 (02/02/2025-02/24/2025) (SWOT 2024a). The HYCOM snapshot is taken during a spring tide on 01/05/2017. While non-linear internal waves are observed in both images, the SWOT data reveal much more submesoscale structure that is not resolved in the HYCOM simulation. A discussion on the dynamics of these nonlinear waves is provided in Buijsman et al. (2025).

The initial deployment phase consists of 50 floats distributed globally (Fig. 1b) operating in a "burst-sampling" mode, making 5 round trip cycles to 2000 m over 2 days (Fig. 5c) with the aim of separating internal waves from other forms of oceanic variability. Between bursts, the floats park at 1000 m depth for 10 days, again similar to the global Argo array. Overall intra-burst variance gives an estimate of the broadband internal wave energy present, and harmonic analysis (Fig. 5e) enables the estimation of narrow-band signals at the dominant frequencies of tide and wind forcing (diurnal, semidiurnal, and the latitude-varying inertial frequency). The 2000 m profiling allows separation of these signals by vertical mode (Fig. 5f). In addition, the high vertical resolution of the profilers facilitates calculation of vertical wavenumber spectra for comparison with internal wave continuum models (e.g., GM76; Garrett and Munk 1975; Cairns and Williams 1976).

SQUID deployments to date have occurred on GO-SHIP large-scale hydrography lines and other cruises of opportunity, including transits and regional process studies. Floats have been launched in all of the world's oceans strong currents including the Gulf Stream and ACC, internal tide beams from Hawai'i, Luzon Strait, and the Mariana Ridge, and in the equatorial regions (Fig. 1b). Though

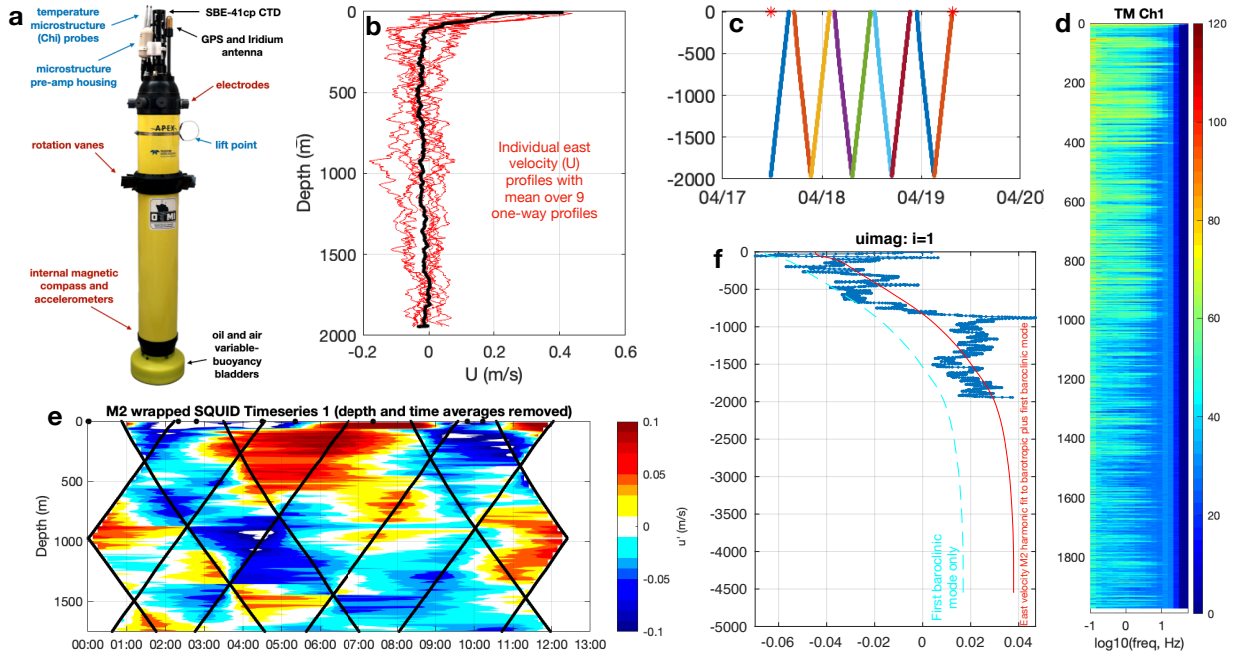

FIG. 5: (a) An EM-APEX profiling float configured as used in the NOPP GIW to collect (b) velocity profiles (east component from one 9-profile "burst") while cycling vertically to 2000 m (c). (d) Example temperature microstructure profile, showing 20-second spectra sent over Iridium. (e) A semidiurnal (M_2)-wrapped view of the velocity profiles in (b), showing the relatively even (though coarse) phase coverage. (f) Illustration of vertical mode fitting to a frequency harmonic—in this case, the sine (imaginary) component of the east velocity timeseries at each depth.

previous internal wave and microstructure measurements have been made in all of these settings, the coordinated approach of a uniform measurement platform and an immediate connection to modeling output and model validation goals makes this new dataset particularly valuable.

Metrics for evaluating the success of the project will include (1) the range of internal wave statistics sampled relative to (2) the considerable uncertainties resulting from the minimal burst sampling and spectral analysis (coarse temporal resolution combined with high vertical resolution). The harmonic phase coverage and frequency separability inherent in the sampling scheme for the semidiurnal, diurnal, and inertial frequencies will result in different levels of uncertainty in different locations. However, the variance outside of each harmonic fit band will help determine the uncertainties in amplitude and phase of the resulting harmonics (particularly the low vertical modes). (3) Direct comparisons between observed internal wave parameters, such as energy flux of the low-mode tidal or near-inertial internal waves, with global models that resolve the wave-generation process and signal-to-noise ratio of the harmonic will be an important facet of model validation, while (4) spectral levels of high-wavenumber shear will aid the refinement of internal

wave based parameterizations for diapycnal mixing (Gregg 1989; Henyey et al. 1986; Polzin et al. 1995; Kunze et al. 2006).

The Distributed Sensor Network for the Ocean's Bottom Boundary Layer

Our Distributed Sensor Network is designed to investigate basic fluid dynamics at the ocean's bottom boundary. This effort is motivated by the lack of ground truth concerning the relative roles of gravity and rotation in determining the structure of the planetary boundary layer and its feedback onto the Earth system behavior. In this venue, data sparseness limits the reliability of ocean model predictions because even the best Ocean Bottom Boundary Layer (OBBL) schemes are simply upside down versions of Ocean Surface Boundary Layer (OSBL) schemes. These schemes ignore the phenomenology associated with sloping bathymetry that couples to critical and near-critical internal waves, and topographic roughness that leads to flow blocking, splitting, separation, and internal hydraulics (Polzin and McDougall 2022). Our efforts are focused upon steep and complex topography where numerical model deficiencies are especially pernicious (Blain et al. 2025).

We achieve high spatial/temporal resolution with a Distributed Sensor Network that is full ocean depth capable and has sub-second sampling rates that enable estimates of turbulent dissipation and three-dimensional (3D) fluxes of mass, momentum and energy in both turbulent and internal wavebands; and provides realizations on multiple fortnightly and mesoscale eddy time scales with year-long deployments. The sensors in our network are based-on scalable, proven technology (Fig. 6). The unique capabilities of the network are arrived at by deploying these sensors in an array that enables us to visualize the phenomenology and quantify the physics of the ocean's bottom boundary layer that have been the source of longstanding ignorance and misunderstanding. In short, our Distributed Sensor Network tries to be a 3D antenna that resolves all, and in particular, coherent features that are especially important to determining the structure of the OBBL.

To date, individual sensor network assets have been used in a downwelling Ekman layer to document wave band motions radiating significant momentum and energy away from the OBBL and to establish that the associated temperature fluxes are a key factor in restratifying the near-boundary region determining planetary boundary layer structure (Polzin et al. 2021). Similarly, sensor network assets have documented highly non-local temperature fluxes associated with internal Kelvin wave seiching in a canyon that, phenomenologically, appear to be the analog of a surface

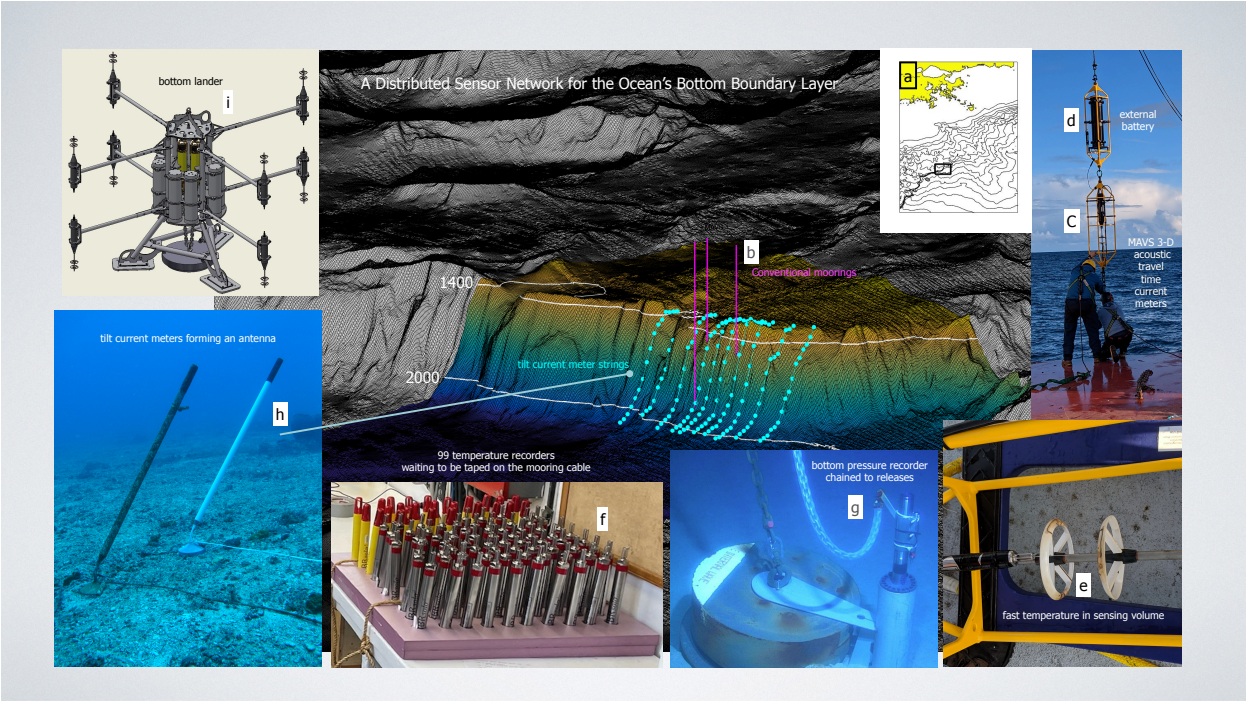

FIG. 6: Distributed Sensor Network assets draped over a steep escarpment in the Gulf of Mexico (a). The sensor network is arranged about one or more conventional taut wire moorings (b) hosting MAVS acoustic travel time current meters (c) that provide estimates of 3D currents, turbulent dissipation through inertial subrange formulas, and fluxes of momentum and buoyancy at time scales of seconds to hours. A single external battery pack (d) enables 6 months of sampling at 5 Hz. A serial streaming temperature recorder with custom 10 cm long string whose tip is placed within the sensing volume of the acoustic current meter (e) provides co-located temperature/velocity measurements. Fifty to one hundred self-contained temperature recorders (f) sampling at 0.5-1.0 Hz for 1 year duration are taped onto the mooring and provide high vertical resolution of internal wave and outer turbulent boundary layers. Direct estimates of energy flux (pressure work) can be obtained by using the temperature recorder data to vertically integrate the hydrostatic relation and placing a bottom pressure recorder in a special frame on the anchor (g) to provide time varying pressure as a function of height above bottom, and then combining these with the 3D currents. Individual Tilt Current Meters (TCMs; h) are self contained units and sample at 8 Hz with a duration of one-year. In the Sensor Network, these units are deployed along lines of 6-10 km length with anchors at either end, but the nominal extent is virtually unlimited. A bottom lander (i) populated by 8 MAVS current meters measuring at 0.5 and 2.5 m height above bottom provides high vertical resolution of the turbulent OBBL, directly quantifying the frictional stress. As described, the Sensor Network is a base that can be complimented by more traditional sensors. In total, the Sensor Network assets return full resolution of turbulent and internal waveband contributions to budgets of momentum, buoyancy, vorticity and energy.

gravity wave shoaling on a beach (Polzin 2025). These realizations provide us with dramatic departures from existing concepts, as discussed in Polzin and McDougall (2022), of the physical mechanisms determining the structure of the ocean's bottom boundary layer.

This Distributed Sensor Network was successfully tested recently on the northern slope of the Gulf of Mexico. A 6×6 km^2 grid consisting of 55 Seahorse Tilt Current meters and a vertical MAVS mooring with an additional 100 thermistors was deployed from July to November 2024. After the successful deployment and recovery cruises, analysis is underway.

b. Model Simulations

In this section we report on (1) advances in simulating tides in the global Modular Ocean Model (MOM6) simulations, (2) the skill of global HYCOM simulations in predicting the energy and phase of the internal tides, (3) improvements in data assimilation and vertical coordinates to mitigate spurious waves, and (4) the necessity of high-resolution regional and process simulations to better resolve internal wave processes.

Global MOM6 Simulations

MOM6 was developed by the Geophysical Fluid Dynamics Laboratory of the National Oceanic and Atmospheric Administration for solving the hydrostatic primitive equations in spherical polar geometry (Adcroft et al. 2019)[2]. The equations of motion are discretized on a horizontal Arakawa C-grid and utilize a realistic equation of state for sea water. In order to minimize the spurious mixing caused by numerical advection algorithms (Griffies et al. 2000; Ilicak et al. 2012), the vertical coordinate of MOM6, as in HYCOM, is Lagrangian for isentropic motions, a feature which distinguishes it from other widely used models, such as MITgcm and ROMS. The evolution of the water column is decomposed into adiabatic and non-adiabatic dynamics which are integrated using the Arbitrary-Lagrangian-Eulerian (ALE) method (White and Adcroft 2008; White et al. 2009; Griffies et al. 2020). The split-explicit time stepping method (Hallberg and Adcroft 2009) and the numerics of the pressure gradient force (Adcroft et al. 2008) are designed to be stable and accurate even in situations with steeply-sloping coordinate surfaces.

Activities with MOM6 in the scope of the NOPP GIW project have included a range of efforts. In order to build confidence in MOM6 as a tool for tide-resolving simulations, the source code was extensively reviewed and a few minor errors in the implementation of tidal forcing were identified and corrected. To facilitate the analysis of simulation outputs, new code modules were developed to implement inline, or run-time, harmonic analysis and the computation of baroclinic sea level diagnostics (Zaron and Ray 2023). To make simulations more realistic, an enhanced (frequency-dependent) parameterization of topographic wave drag was implemented to represent the effects of unresolved waves from either subgrid-scale topography or insufficient vertical resolution (Xu and Zaron 2024). The new wave drag implementation enables the use of different latitude-

[2]Ongoing development of MOM6 is being carried out by a large community consortium under an open development paradigm, `https://github.com/mom-ocean/MOM6`.

dependent drag coefficient fields for the diurnal and semi-diurnal frequency bands, separately from the parameterizations designed to affect the low-frequency mesoscale flows (Xu and Zaron 2025). Finally, all these features have been utilized to conduct MOM6 simulations on a global tripolar grid with nominal $1/12.5^\circ$ horizontal resolution and 41 hybrid layers, similar to HYCOM, bringing MOM6 tidal simulations into approximate parity with the HYCOM-based simulations developed inside the U.S. Navy.

A series of global MOM6 simulations have been conducted to optimize the wave drag parameterization for the main semidiurnal and diurnal tidal constituents, M_2 and K_1. Comparisons of two-dimensional (2D; barotropic dynamics) and 3D (combined barotropic and baroclinic dynamics) simulations reveal the significant role of topographically-trapped sub-inertial waves at high latitudes, leading to more accurate results for the K_1 tide than previously obtained with global models (Figs. 7 and 8). Comparisons with satellite altimetry (TPXO9; Egbert and Erofeeva 2002)) find globally-averaged root-mean-square errors of 2.35 cm and 0.85 cm, respectively, for M_2 and K_1, which are among the best accuracies for non-data-assimilative global simulations (Xu and Zaron 2025). The predicted baroclinic sea level also shows promising agreement with an altimeter-derived estimate (High Resolution Empirical Tides (HRET8.1); Zaron 2019b), but the evaluations are more complex owing to the dependence of these waves on the large-scale stratification. The chief factors contributing to the model's accuracy are the new wave drag parameterization and bottom topography on the tripolar grid, which has been adapted from NOAA's Global Surge and Tide Operational Forecast System (NOAA 2023).

Global HYCOM Simulations

A major goal of NOPP GIW is to assess and improve the predictability of internal tides in the HYbrid Coordinate Ocean Model, which is the dynamical core of the U.S. Navy Global Ocean Forecasting System (GOFS). To obtain accurate operational forecasts of geostrophically balanced motions, observational data is assimilated in HYCOM with the Navy Coupled Ocean Data Assimilation 3D Variational Analysis (NCODA-3DVar) System (Chassignet et al. 2009; Cummings and Smedstad 2013). Moreover, due to the inclusion of high resolution bathymetry and optimized SAL and wave-drag parameterizations, HYCOM has also become the state of the art in

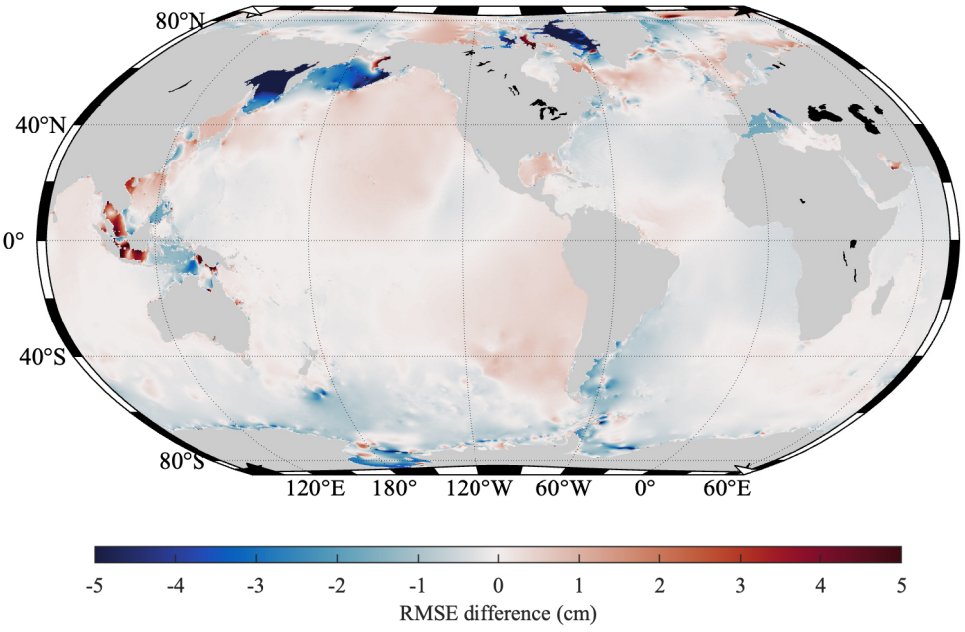

FIG. 7: Differences in the RMSE of K_1 barotropic tidal elevation between the 3D and 2D MOM6 simulations, compared with the altimeter-derived TPXO9 model. Negative values (blue) indicate more accurate representations of the tidal elevations in the 3D simulation. Improved accuracies in these regions highlight the significance of topographically-trapped baroclinic waves resolved in high-resolution 3D MOM6 simulations.

predicting accurate surface and internal tides when compared to other global ocean models (Arbic 2022).

Comparing HYCOM's internal tide SSH with satellite altimetry provides a direct way to assess its skill globally. In this aspect of our work, we set out to evaluate the skill of $1/25^\circ$ HYCOM against three altimetric datasets: (1) nadir altimetry (JASON), (2) the Calibration/Validation (Cal/Val) period of the first wide-swath altimeter (SWOT), and (3) the SWOT science orbit. Previous studies (Carrère et al. 2021) have shown that non-data-assimilative HYCOM solutions are less effective at removing internal tide SSH variance from classical nadir altimeter records than empirical internal tide models because of mismatches between the predicted and observed ocean circulation. However, in Yadidya et al. (2024) we investigated the phase accuracy of a data-assimilative, tide-resolving HYCOM forecast system and found that it removes internal tide SSH variance from nadir altimetry at skill levels comparable to the state-of-the-art empirical correction model HRET8.1 (Fig. 9).

Internal tide prediction consists of both coherent (phase-locked) and incoherent (non-phase-locked) components. While empirical models based on nadir altimetry, such as HRET8.1, can

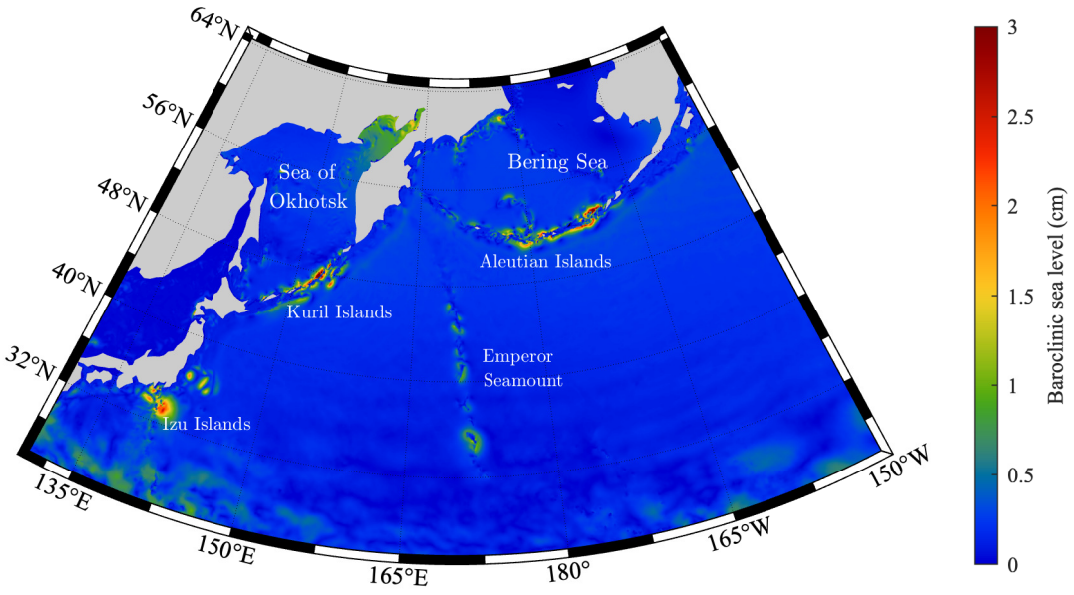

FIG. 8: Amplitude of baroclinic sea level associated with the K_1 tide in the north Pacific shows the scale of the topographically-trapped subinertial waves resolved in 3D MOM6 simulations. The mixing caused by these waves is hypothesized to be a significant control on water mass properties and thus influences large-scale non-tidal dynamics.

only predict the coherent signal, HYCOM offers the opportunity to also capture the incoherent component. Yadidya et al. (2024) demonstrates that HYCOM captures up to 14.7% more internal tide SSH variance in nadir altimeter records when both incoherent and coherent components are considered, relative to the performance when only the coherent component is considered, as in Fig. 9b. Preliminary results from SWOT Cal/Val and science orbits also indicate that HYCOM removes up to 9% more coherent internal tide SSH variance than HRET8.1 and an additional 15% more incoherent variance. These results indicate that forecast models such as HYCOM offer a novel approach for improving global internal tide mapping and altimetry corrections. Furthermore, because HYCOM explicitly represents the full water column, it serves as a valuable tool for advancing our understanding of internal tide dynamics.

Improvements in Data Assimilation and Vertical Coordinates

While the NCODA-3DVAR data assimilation has significantly improved HYCOM's predictive capabilities for ocean circulation over a wide range of frequencies and wavenumbers, it is not

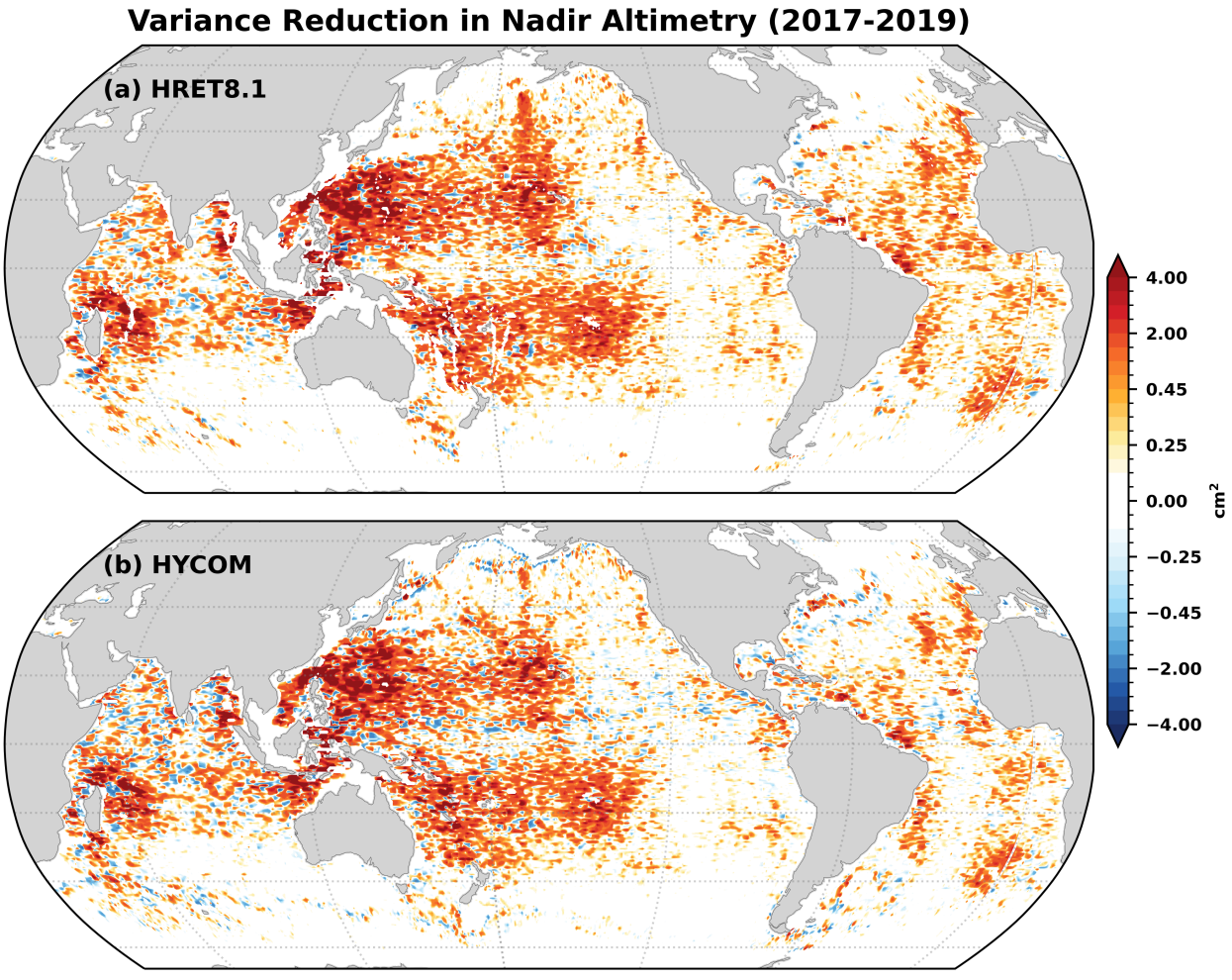

FIG. 9: Global maps of internal tide SSH variance reduction in nadir altimetry by (a) HRET8.1 and (b) 1/25° HYCOM. The HYCOM results come from a three-year harmonic analysis of total SSH after applying a Gaussian spatial filter to extract the coherent internal tide signal. Adapted from Yadidya et al. (2024).

without drawbacks. The data assimilation procedure causes shocks in the positioning of mesoscale fields and these shocks can result in spurious high-frequency internal waves in regions with strong mesoscale activity. These spurious internal waves cause an excess of energy when compared to observations (drifters) and/or to simulations without data assimilation. We have been quantifying the improvements in predictions that can be obtained with either a better choice of data assimilation parameters (e.g., initialization, vertical projection, covariance, time windows, etc.) in the existing 3DVAR systems where all ocean variables are analyzed simultaneously in three dimensions, or adoption of more sophisticated data assimilation techniques such as the four-dimensional variational

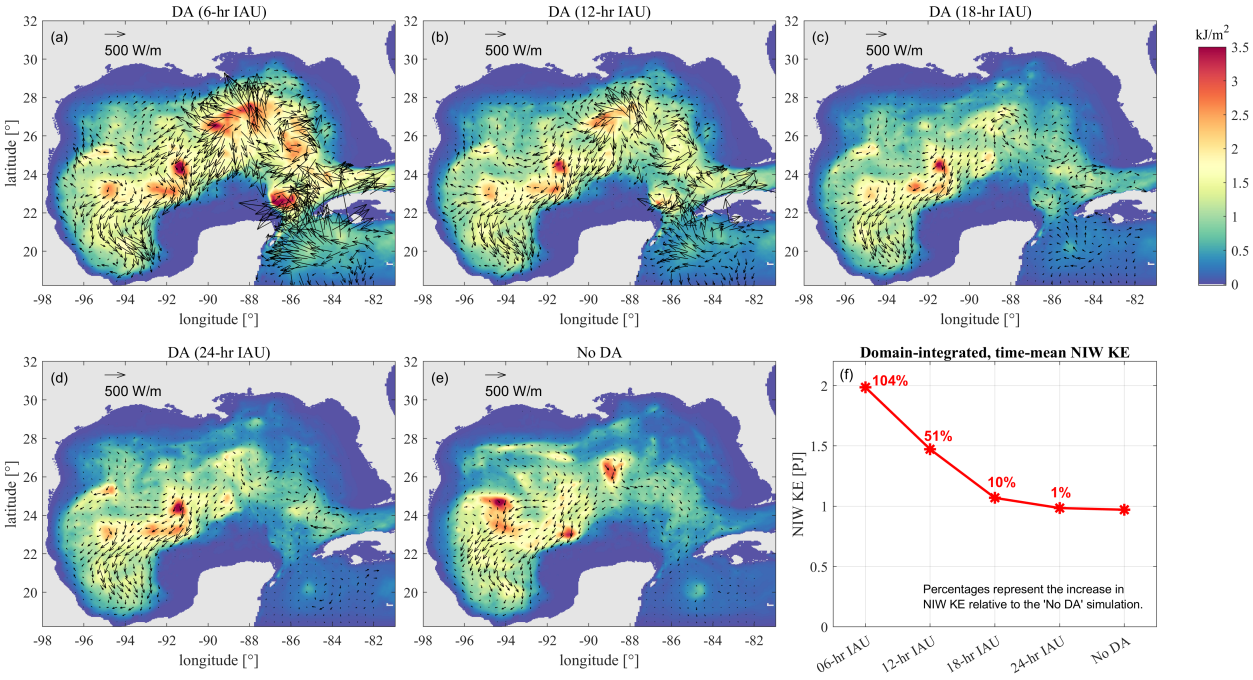

FIG. 10: The depth-integrated, time-mean NIW kinetic energy (color) and horizontal energy fluxes (vectors) in the Gulf of Mexico in simulations with (a) 6-h, (b) 12-h, (c) 18-h and (d) 24-h IAU, and (e) no DA. (f) Domain-integrated, time averaged NIW kinetic energy in the Gulf of Mexico regional simulations with different IAU periods.

(4DVAR; Weaver 2003) and the local ensemble transform Kalman filter (LETKF; see Martin et al. 2025, for a recent review of the state of the art in data assimilation schemes for ocean forecasting).

Raja et al. (2024) demonstrate that the spurious near-inertial internal waves, generated during data updates, can be effectively mitigated by introducing smaller increments over multiple time steps during data updates, a process achieved by extending the Incremental Analysis Update (IAU) period. The impact of different IAU periods on spurious near-inertial wave (NIW) generation was evaluated using a regional HYCOM configuration in the Gulf of Mexico, with data assimilation performed using the open-source Tendral Statistical Interpolation System (TSIS) developed by Srinivasan et al. (2022). Extending the IAU period to 24 hours reduces spurious energy to 1% of NIW kinetic energy (Fig. 10), significantly improving the model's fidelity in representing internal waves.

The 4DVAR methodology provides a dynamically balanced analysis by expanding the background error covariance used by the 3DVAR method to a fourth dimension (time) via the tangent linear and adjoint of the forward model operator. The tangent linear and adjoint are used to compute

derivatives of the model outputs with respect to the input parameters which are required in the minimization process between the observations and the numerical model. Due to its time-varying vertical coordinate, the HYCOM numerical implementation does not lend itself to adequate linearization and adjoint development. We have worked with the assumption that one can use the tangent linear and adjoint of another ocean model as a proxy for the operators of HYCOM, and we have developed the capability to use the NCOM-4DVAR, a 4DVAR system for the U.S. Navy Coastal Ocean Model (NCOM; Ngodock and Carrier 2014) as a proxy ocean data assimilation system for HYCOM. Over a short time period (about 120 hours), a NCOM forecast is close to a HYCOM forecast if given the same initial and boundary condition states, as well as the atmospheric forcing. We have carried out a month-long numerical experiment in the Gulf of Mexico, where analysis increments are computed from the NCOM-4DVAR and added to a HYCOM forecast to make a HYCOM analysis. This HYCOM analysis is then used to initialize a new HYCOM forecast and so on. A time series comparison of analysis residuals from the existing 3DVAR and the new proxy 4DVAR for HYCOM is shown in Fig. 11, for both temperature and salinity. The residuals are computed as daily root mean square errors against assimilated *in situ* profiles. It can be seen in Fig. 11 that the proxy HYCOM 4DVAR produces an analysis that has significantly lower errors than the existing 3DVAR. These lower analysis errors also result in lower forecast errors (not shown). We are in the process of evaluating the amount of spurious internal waves generated by this proxy HYCOM 4DVAR approach.

Finally, another source of noise in HYCOM is thermobaric instabilities arising from the thermobaricty correction (Sun et al. 1999) used in the σ_2 potential density gradient calculation. This correction can be unstable (Hallberg 2005) if (a) temperature and salinity are far from their reference state, which is from the Atlantic, or (b) stratification is low, i.e., isopycnal layers are thick. In the standard 41-layer global setup, layer 36 is more than 2000 m thick in the high latitude North Pacific and it leads to thermobaric instability in this region (Buijsman et al. 2016, 2020; Raja et al. 2022). This numerical noise mostly projects on shorter wavelength internal waves, such as high-mode semidiurnal internal waves and all modes with supertidal frequencies > 2 cycles per day (Buijsman et al. 2025). Hence, the noise does not exist in the mode-1 fields in Fig. 1. We have found that the instability can be completely removed by splitting layer 36 into several layers, which can be achieved by adding new layers or by setting the maximum layer thickness to 750 m.

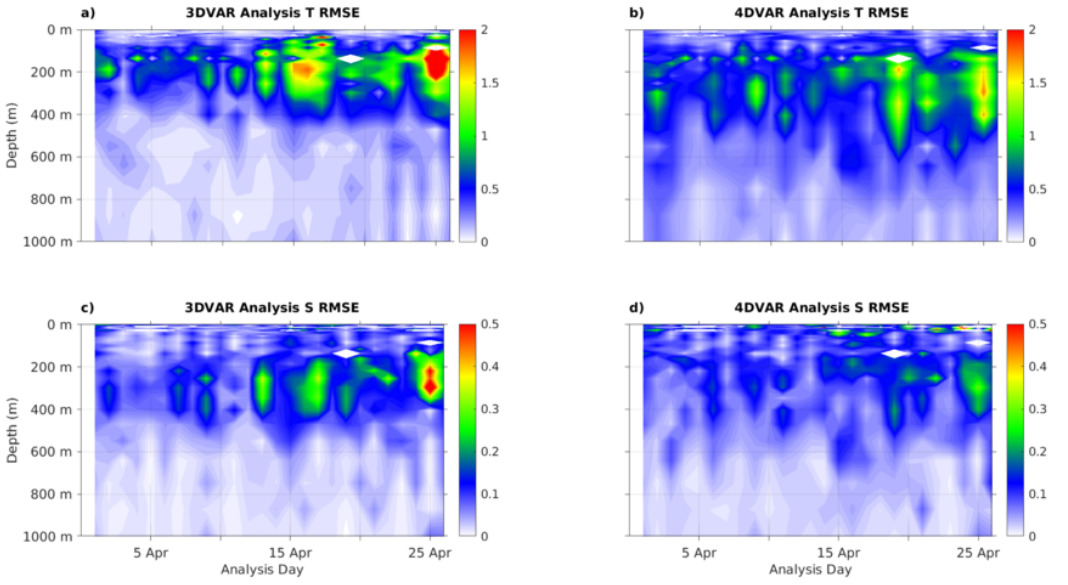

FIG. 11: A comparison of HYCOM daily analysis root mean square errors from both 3DVAR and the proxy 4DVAR. Errors are for (a) 3DVAR temperature, (b) proxy 4DVAR temperature, (c) 3DVAR salinity, and (d) proxy 4DVAR salinity.

REGIONAL AND PROCESS MODEL SIMULATIONS

While the grid resolution of global simulations with tides has increased during the last decades, their resolution is not yet sufficient to accurately simulate internal-wave processes at the continental margins, or to resolve the high-frequency internal wave spectrum in either the coastal or open ocean. Hence, it is necessary to perform coastal regional simulations, or simulations with a more developed internal wave spectrum, with a higher resolution. To obtain realistic internal wave energy levels, however, these regional simulations need to be forced not only with surface tides and mesoscale flows, but also with remote internal wave forcing at the boundaries (Mazloff et al. 2020; Nelson et al. 2020). To study the effect of remote waves along the U.S. Westcoast, we have forced $1/25°$ Regional Ocean Modeling System (ROMS; Shchepetkin and McWilliams 2005) simulations with surface tides and (super)tidal internal waves from a global $1/12.5°$ HYCOM simulation (Siyanbola et al. 2023, 2024). Internal tides generated near Hawai'i (Fig. 1) greatly increase the semidiurnal internal tide fluxes in the regional model with remote forcing (Fig. 12).

With our regional and process-study modeling simulations, we have focused on quantifying which internal-wave processes are underestimated or overestimated when the horizontal gridspacing is

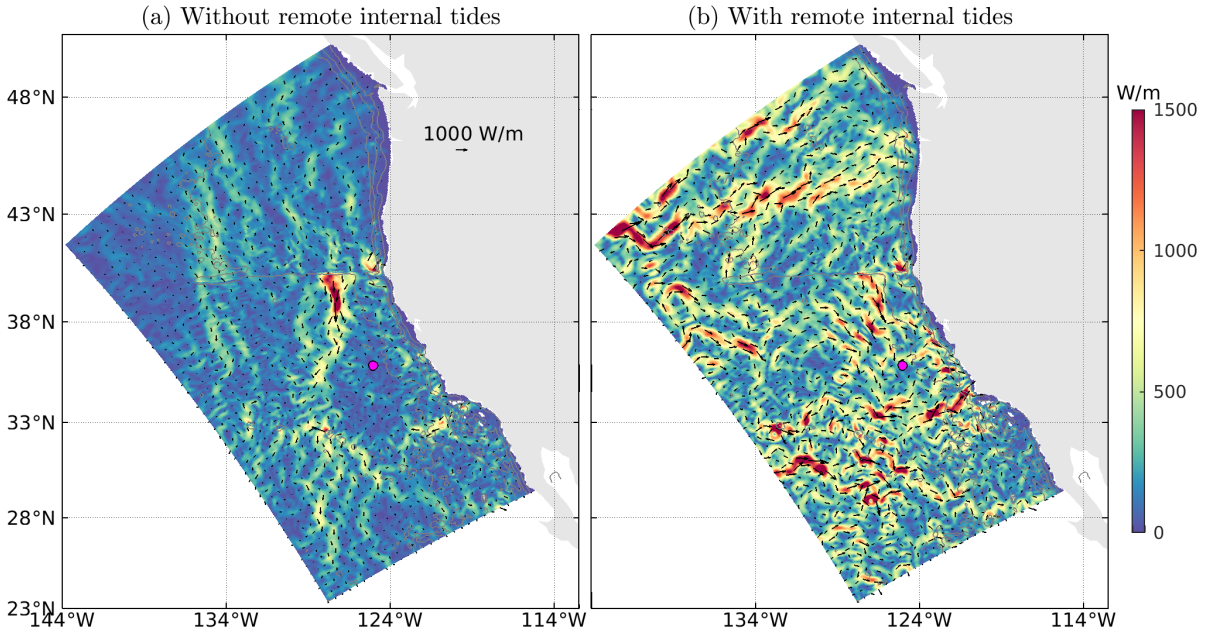

FIG. 12: Depth-integrated and time-mean (01 July - 31 August, 2012) semidiurnal band (1.60-2.67 cycles per day) internal wave energy fluxes for (a) a ROMS simulation without and (b) a ROMS simulation with remote internal tide forcing from a global HYCOM simulation (Siyanbola et al. 2023). The gray contours mark the 2000 and 4000 seafloor depths. The magenta-filled circle marks the IWR array location.

decreased to $O(1\text{ km})$. A suite of regional simulations of the Brazilian Basin with different grid resolutions, with and without tidal forcing (Huang et al. 2025, submitted), have revealed significant departures from the observational literature (e.g., Polzin et al. 1997) in the relative role played by submesoscale circulations and internal waves. Ocean models run at kilometer-scale resolution predict observed diapycnal diffusivity values, but the process modulating the energy and buoyancy exchanges around steep topography is vorticity generation/intensification rather than wave dynamics, as observed. This occurs because, even at such high resolution of $O(1\text{ km})$, the topography remains too smooth to block and scatter internal tides, limiting wave breaking. An example of internal wave breaking along steep topography in an idealized large eddy simulation (LES) can be seen in Fig. 13c, where wave breaking leads to lateral intrusions with vertical height set by the ratio of wave velocity to interior stratification, U_w/N. , transporting mixed-waters from the boundary into the interior (Whitley and Wenegrat 2025). These processes are absent at lower resolution, with impacts that can be framed in terms of the differences between the modeled and

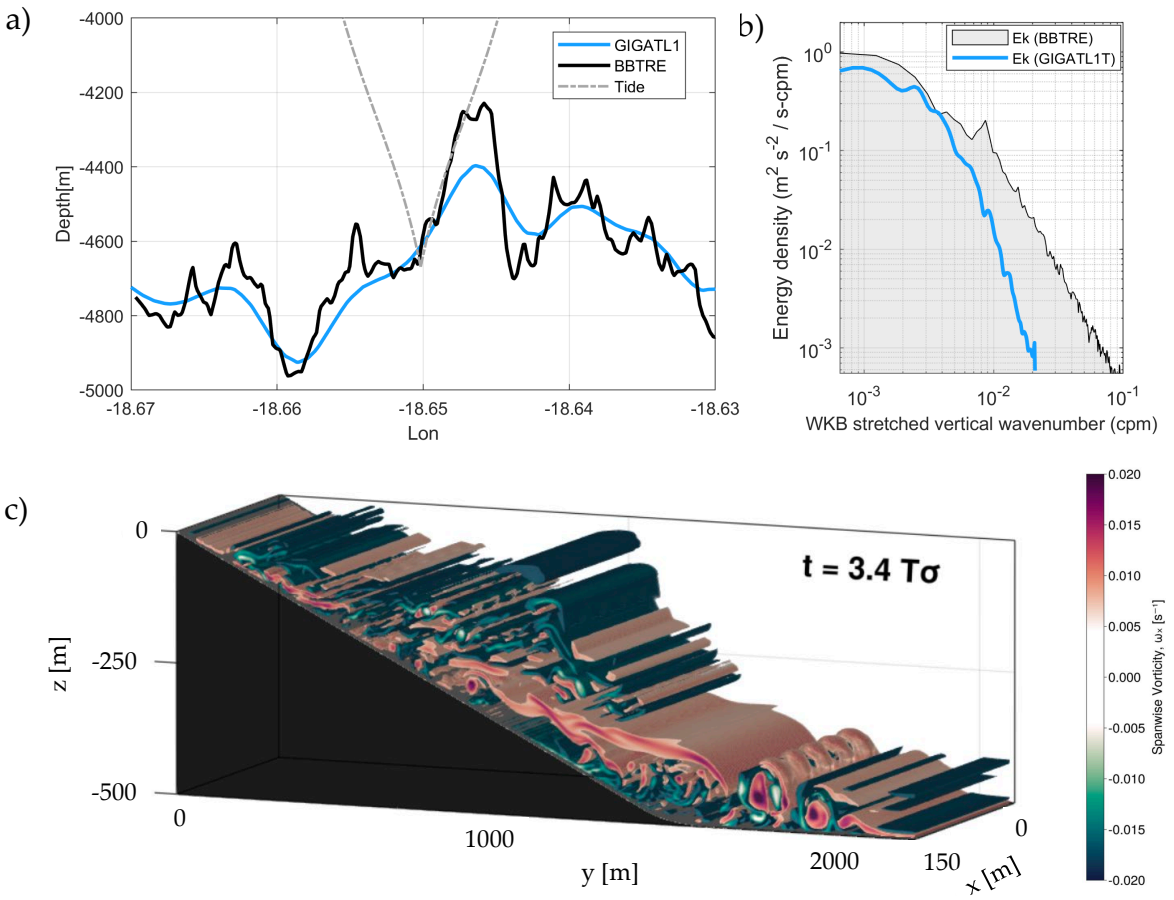

FIG. 13: (a) Topography along a transect in the Brazilian Basin as measured during the Brazilian Basin Tracer Release Experiment (BBTRE) and in a ROMS simulation at 1 km horizontal resolution (Gula et al. 2021). An example of internal wave ray trajectory at semi-diurnal frequency is shown in dashed gray. (b) Stretched vertical wavenumber spectra of horizontal kinetic energy (Ek) in the ROMS simulation and BBTRE data. (c) Snapshot of spanwise vorticity from LES of a mode-1 wave breaking at supercritical topography (adapted from Whitley and Wenegrat 2025).

observed topographic height spectrum (Fig. 13a). Those differences result in a divergence between model outputs and observations in the way the energy is transferred in the system (Fig. 13b).

3. Outlook

In this paper we have presented a snapshot of our advances in understanding and predicting the life cycle of internal waves as part of the NOPP GIW project. In what remains, we provide our perspective regarding future developments in observing, simulating, and understanding the internal wave life cycle.

A major unresolved challenge in global ocean modeling is capturing the wide range of spatial and temporal scales associated with internal wave processes. This challenge is partially addressed by ongoing advances in computing hardware, which enable the use of finer vertical and horizontal grid resolutions. For example, global MITgcm simulations have been run at $1/48^\circ$ resolution (Rocha et al. 2016), and a future NOPP-funded project will include a global HYCOM simulation at $1/50^\circ$ resolution. Doubling resolution takes $8\times$ the computing power, or $16\times$ if the number of layers is also doubled. A particularly promising development is the use of Graphics Processing Units (GPUs) which can offer more performance per dollar over traditional Central Processing Units (CPUs). Porting existing models to GPUs may be possible, but relies heavily on advanced compilers. Oceananigans.jl[3] is a new general circulation model explicitly designed to run on GPUs (Ramadhan et al. 2020; Wagner et al. 2025). This nonhydrostatic model, built on the MITgcm framework, has the potential to serve as a high-resolution global ocean modeling platform.

Despite advances toward higher resolution in global and regional Reynolds-averaged numerical simulations (RANS), these models will not resolve internal wave breaking and the associated mixing processes in the foreseeable future. To better capture the forward energy cascade, large-eddy simulations (LES) can be nested within high-resolution regional RANS models (e.g., the Stratified Ocean Model with Adaptive Refinement, SOMAR; Chalamalla et al. 2017). This introduces the technical challenge of bridging intermediate grid scales where turbulence is permitted but not adequately resolved—a regime known as the "gray zone"—a well-known issue in atmospheric modeling (Chow et al. 2019). We have begun evaluating strategies for navigating the gray zone, focusing on the sensitivity of both mean-state and turbulence statistics to closure parameterizations (Chen et al. 2025). Early results provide guidance for effective model nesting across the gray zone and suggest that true multi-scale internal wave modeling is increasingly within reach.

From an operational modeling perspective, generating skillful hour-by-hour forecasts across the global ocean requires not only accurate statistical representations of the internal wave field, but also correct amplitudes and phases of its dominant tidal constituents. Within the internal tide band, this depends on accurately simulating the primary forcing: the surface tide. We show that applying a frequency-dependent wave drag parameterization improves the accuracy of simulated surface tides. Another approach to enhancing surface tide predictability is barotropic nudging, in

[3] https://clima.github.io/OceananigansDocumentation/v0.6.2/benchmarks/?utm_source=chatgpt.com

which the model tides are nudged toward altimetry-constrained solutions (e.g., Fu et al. 2021); this technique is currently being tested in $1/12.5^\circ$ HYCOM simulations.

In parallel, simulating the evolving internal wave field requires assimilation of both phase and amplitude across the internal wave continuum into forecast models, which in turn demands continued advances in data assimilation (DA) techniques. Efforts are underway to reduce DA-related noise and to evaluate the performance of four-dimensional variational (4DVAR) methods at global scales.

The emergence of machine learning (ML; Rumelhart et al. 1986) is increasingly impacting many areas of ocean science (Bracco et al. 2025), including the simulation and observation of internal waves. ML tools have been adopted for a range of applications: data reconstruction and down-scaling (e.g., Martin et al. 2024), subgrid-scale parameterization development, enhancement or replacement of data assimilation methods, pattern recognition and feature tracking (e.g., identifying solitary waves in synthetic aperture radar images; Santos-Ferreira et al. 2025), and the integration of models and observations for data-driven prediction and forecasting (e.g., Zhang et al. 2021). While most forecasting applications to date have been limited to regional scales, such approaches may offer promising new pathways for characterizing global internal tide energy fields and their interactions (Liu et al. 2025).

Finally, improved observational techniques, strategies, and investments will also be necessary in order to advance towards accurate internal wave representation in forecast models. Parameterized processes like ocean mixing need to be constrained on a global scale. Recent technological advances on ocean turbulence observations are comprehensively summarized in Frajka-Williams et al. (2022). Moreover, recent innovations including instrumentation on ocean platforms such as floats (e.g., Moum et al. 2023), drifting surface platforms (e.g., Zeiden et al. 2024), underwater gliders (e.g., Carlson et al. 2025), and moorings (e.g., Miller et al. 2023; Whitwell et al. 2024) also hold great promise. New remote sensing techniques (e.g., Spence et al. 2024), distributed networks of sensors (e.g., Pelaez Quiñones et al. 2023) and distributed measurements using sub-sea fiber optic cables (e.g., Sinnett et al. 2020; Lucas and Pinkel 2022) are all beginning to capture the details of the 4D processes that control the forward cascade of energy from the internal wave continuum to turbulence and mixing. Comparisons of the internal wave dissipation in high-resolution global and regional models with rates inferred from turbulence observations indicate that the internal wave

models discussed here are starting to show some skill in directly simulating internal wave mixing (Skitka et al. 2024a).

At the global scale, observational networks should be encouraged to make measurements that resolve the internal wave field, through the combination of novel moorings like the system described here, a renewed focus of highly resolved subsurface observations and high-resolution satellite observations such as SWOT SSH which with wide swath start to resolve highly detailed spatial structures of the global propagation of internal waves (e.g., Fig. 4). Concurrent and collaborative improvements in model DA approaches will be necessary for these global observations to improve global forecast models in the internal wave band.

Acknowledgments. J. Wang is supported by NASA grant 80NSSC25K7870. J. Girton and A. Moulin are supported by NSF grant OCE-2232796. Z. Chen, V. Whitley, and J. Wenegrat are supported by NSF grant OCE-2232441. M. Buijsman, D. Varma, B.K. Arbic, and B. Yadidya are funded by ONR grant N0014-22-1-2576. M. Buijsman and O. Siyanbola are supported by NSF grant OCE-1851397. E. D. Zaron and C. Xu are supported by NOAA grant NA22OAR0110487. E. Chassignet. K. Raja, A. Wallcraft, and M. Abdulfatai are supported by ONR grant N0014-22-1-2574. Y. Huang and A. Bracco are supported by NSF grant OCE-2232440. J. Shriver acknowledges support from ONR grant N00014-24-WX0-1587-01. This is NRL contribution NRL/JA/7320-25-XXXX and has been approved for public release. A. F. Waterhouse, A. J. Lucas, U. Send, M. Lankhorst, G. Meiners and C. Griffin are funded by ONR grant N00014-22-1-2575.

Data availability statement. The first 1.5 years of SQUID profiling float data are available at `https://www.ncei.noaa.gov/archive/accession/0305618`. The MOM6 source code is available at `https://github.com/NOAA-GFDL/MOM6`; input data files for re-creating the MOM6 simulations used here are associated with `https://doi.org/10.5281/zenodo.15759343`. Diagnosed energy terms from the ROMS simulations of the U.S. Westcoast are available on `https://doi.org/10.5281/zenodo.7194957`. The semidiurnal and near-inertial fields of modal energy terms for the 1/25° global HYCOM simulation are available on `https://doi.org/10.5281/zenodo.6643378` and `https://doi.org/10.5281/zenodo.5765438`, respectively. Global maps of internal tide SSH variance reduction in nadir altimetry can be reproduced using Yadidya (2023). The data shown in Fig. 3 from the IWR array mooring is publicly available from NASA PO.DAAC (Physical Oceanography Distributed Active Archive Center) at `https://doi.org/10.5067/SWTPO-MOOR2`. The SWOT data used in Fig. 4 can be accessed from PO.DAAC following `https://podaac.jpl.nasa.gov/dataset/SWOT_L2_LR_SSH_2.0`.

References

Adcroft, A., R. Hallberg, and M. Harrison, 2008: A finite volume discretization of the pressure gradient force using analytic integration. *Ocean Modelling*, **22 (3)**, 106–113, https://doi.org/https://doi.org/10.1016/j.ocemod.2008.02.001.

Adcroft, A., and Coauthors, 2019: The gfdl global ocean and sea ice model om4.0: Model description and simulation features. *Journal of Advances in Modeling Earth Systems*, **11 (10)**,

3167–3211, https://doi.org/https://doi.org/10.1029/2019MS001726.

Alford, M. H., 2003: Redistribution of energy available for ocean mixing by long-range propagation of internal waves. *Nature*, **423 (6936)**, 159–162.

Arbic, B. K., 2022: Incorporating tides and internal gravity waves within global ocean general circulation models: A review. *Progress in Oceanography*, **206**, 102 824, https://doi.org/https://doi.org/10.1016/j.pocean.2022.102824.

Arbic, B. K., S. T. Garner, R. W. Hallberg, and H. L. Simmons, 2004: The accuracy of surface elevations in forward global barotropic and baroclinic tide models. *Deep-Sea Research II*, **51**, 3069–3101.

Arbic, B. K., A. J. Wallcraft, and E. J. Metzger, 2010: Concurrent simulation of the eddying general circulation and tides in a global ocean model. *Ocean Modelling*, **32**, 175–187, https://doi.org/10.1016/j.ocemod.2010.01.007.

Archer, M., J. Wang, P. Klein, G. Dibarboure, and L.-L. Fu, 2025: Wide-swath satellite altimetry unveils global submesoscale ocean dynamics. *Nature*, **(640)**, 691–696, https://doi.org/10.1038/s41586-025-08722-8.

Blain, C. A., Z. Yu, and T. R. Campbell, 2025: Sea bottom warfare: Predicting deep ocean currents in the south china sea. Tech. Rep. NRL Memorandum Report IR-7232-25-2-U (submitted), Naval Research Laboratory, Washington, DC.

Bleck, R., 2002: An oceanic general circulation model framed in hybrid isopycnic cartesian coordinates. *Ocean Modelling*, **4**, 55–88, https://doi.org/10.1016/S1463-5003(01)00012-9.

Boegman, L., and M. Stastna, 2019: Sediment resuspension and transport by internal solitary waves. *Annual Review of Fluid Mechanics*, **51**, 129–154.

Bracco, A., J. Brajard, H. A. Dijkstra, P. Hassanzadeh, C. Lessig, and C. Monteleoni, 2025: Machine learning for the physics of climate. *Nature Reviews Physics*, **7 (1)**, 6–20, https://doi.org/10.1038/s42254-024-00776-3.

Briscoe, M. G., 1975: Internal waves in the ocean. *Rev. Geophys.*, **13 (3)**, 591–598.

Buijsman, M., and Coauthors, 2016: Impact of parameterized internal wave drag on the semidiurnal energy balance in a global ocean circulation model. *Journal of Physical Oceanogry*, **46**, 1399–1419, https://doi.org/10.1175/JPO-D-15-0074.1.

Buijsman, M. C., B. K. Arbic, J. Green, R. W. Helber, J. G. Richman, J. F. Shriver, P. Timko, and A. Wallcraft, 2015: Optimizing internal wave drag in a forward barotropic model with semidiurnal tides. *Ocean Modelling*, **85**, 42–55.

Buijsman, M. C., B. K. Arbic, S. M. Kelly, and A. F. Waterhouse, 2019: *Internal gravity waves*. Third edition ed., Academic Press, Oxford, 622–632 pp., https://doi.org/10.1016/B978-0-12-409548-9.04160-9.

Buijsman, M. C., and Coauthors, 2020: On the interplay between horizontal resolution and wave drag and their effect on tidal baroclinic mode waves in realistic global ocean simulations. *Ocean Modelling*, **152 (101656)**, https://doi.org/10.1016/j.ocemod.2020.101656.

Buijsman, M. C., and Coauthors, 2025: Energetics of (super)tidal baroclinic modes in a realistically forced global ocean simulation. *Journal of Geophysical Research: Oceans*, **130 (e2025JC022460)**, https://doi.org/10.1029/2025JC022460.

Cairns, J. L., and G. O. Williams, 1976: Internal wave observations from a midwater float, 2. *Journal of Geophysical Research*, **81**, 1943–1950, https://doi.org/10.1029/jc081i012p01943.

Carlson, D., L. Merkelbach, and J. Carpenter, 2025: Measuring ocean turbulence under extreme storm conditions using helicopter-deployed ocean gliders. Tech. rep., Copernicus Meetings.

Carrère, L., and Coauthors, 2021: Accuracy assessment of global internal-tide models using satellite altimetry. *Ocean Sciences*, **17**, 147–180, https://doi.org/https://doi.org/10.5194/os-17-147-2021.

Chalamalla, V. K., E. Santilli, A. Scotti, and S. Sarkar, 2017: Somar-les: A framework for multi-scale modeling of turbulent stratified oceanic flows. *Ocean Modelling*, **120**, 101–119, https://doi.org/10.1016/j.ocemod.2017.11.003.

Chassignet, E., and Coauthors, 2009: U.s. godae: Global ocean prediction with the HYbrid Coordinate Ocean Model (HYCOM). *Oceanography*, **22 (2)**, 64–75.

Chen, S.-T., D.-J. Li, H. Tian, J.-Y. Hou, D.-Y. Ning, and Y.-J. Gong, 2022: Experimental study of the effect of internal waves on the rotational hydrodynamics of underwater vehicle. *International Journal of Naval Architecture and Ocean Engineering*, **14**, 100 465.

Chen, Z., J. Wenegrat, T. Chor, and P. Marchesiello, 2025: Evaluating Turbulence Parameterizations at Gray Zone Resolution for the Ocean Surface Boundary Layer. *in review for JAMES*.

Chow, F., C. Schar, N. Ban, K. Lundquist, L. Schlemmer, and X. Shi, 2019: Crossing Multiple Gray Zones in the Transition from Mesoscale to Microscale Simulation over Complex Terrain. *Atmosphere*, **10 (5)**, 274, https://doi.org/10.3390/atmos10050274.

Colosi, J. A., 2016: *Sound propagation through the stochastic ocean*. Cambridge University Press.

Cummings, J. A., and O. M. Smedstad, 2013: Variational data assimilation for the global ocean. *Data Assimilation for Atmospheric, Oceanic and Hydrologic Applications, S. K. Park and L. Xu, Eds., Springer-Verlag*, **II**, 303–343.

Egbert, G. D., and S. Y. Erofeeva, 2002: Efficient inverse modeling of barotropic ocean tides. *jtech*, **19**, 183–204.

Egbert, G. D., and R. D. Ray, 2000: Significant tidal dissipation in the deep ocean inferred from satellite altimeter data. *Nature*, **405**, 775–778.

Flexas, M. M., A. F. Thompson, H. S. Torres, P. Klein, J. T. Farrar, H. Zhang, and D. Menemenlis, 2019: Global estimates of the energy transfer from the wind to the ocean, with emphasis on near-inertial oscillations. *Journal of Geophysical Research: Oceans*, **124 (8)**, 5723–5746, https://doi.org/https://doi.org/10.1029/2018JC014453.

Frajka-Williams, E., J. A. Brearley, J. D. Nash, and C. B. Whalen, 2022: Chapter 14 - new technological frontiers in ocean mixing. *Ocean Mixing*, M. Meredith, and A. Naveira Garabato, Eds., Elsevier, 345–361, https://doi.org/https://doi.org/10.1016/B978-0-12-821512-8.00021-9, URL https://www.sciencedirect.com/science/article/pii/B9780128215128000219.

Fu, H., X. Wu, W. Li, L. Zhang, K. Liu, and B. Dan, 2021: Improving the accuracy of barotropic and internal tides embedded in a high-resolution global ocean circulation model of mitgcm. *Ocean Modelling*, **162**, 101 809, https://doi.org/https://doi.org/10.1016/j.ocemod.2021.101809.

Furuichi, N., T. Hibiya, and Y. Niwa, 2008: Model-predicted distribution of wind-induced internal wave energy in the world's oceans. *Journal of Geophysical Research: Oceans*, **113 (C9)**, https://doi.org/https://doi.org/10.1029/2008JC004768.

Garrett, C., and W. Munk, 1979: Internal waves in the ocean. *Annual Review of Fluid Mechanics*, **11**, 339–369, https://doi.org/https://doi.org/10.1146/annurev.fl.11.010179.002011.

Garrett, C. J. R., and W. H. Munk, 1975: Space-time scales of internal waves. A progress report . *Journal of Geophysical Research*, **80**, 291—-297, https://doi.org/10.1029/JC080i003p00291.

Gill, A. E., 1982: *Atmosphere-ocean dynamics*, Vol. 30. Academic Press.

Gregg, M. C., 1989: Scaling turbulent dissipation in the thermocline. *Journal of Geophysical Research*, **94**, 9686–9898, https://doi.org/10.1029/JC094iC07p09686.

Griffies, S. M., A. Adcroft, and R. W. Hallberg, 2020: A primer on the vertical Lagrangian-remap method in ocean models based on finite volume generalized vertical coordinates. *james*, **12**, e2019MS001 954.

Griffies, S. M., R. C. Pacanowski, and R. W. Hallberg, 2000: Spurious diapycnal mixing associated with advection in a z-coordinate ocean model. *mwr*, **128 (3)**, 538–564.

Gula, J., S. Theetten, G. Cambon, and G. Roullet, 2021: Description of the gigatl simulations. Zenodo, https://doi.org/10.5281/ZENODO.4948523.

Hallberg, R., 2005: A thermobaric instability of lagrangian vertical coordinate ocean models. *Ocean Modelling*, **8 (3)**, 279–300, https://doi.org/10.1016/j.ocemod.2004.01.001.

Hallberg, R. W., and A. J. Adcroft, 2009: Reconciling estimates of the free surface height in lagrangian vertical coordinate ocean models with mode-split time stepping. *Ocean Modelling*, **29**, 15–26.

Headrick, R. H., and Coauthors, 2000: Acoustic normal mode fluctuation statistics in the 1995 SWARM internal wave scattering experiment. *The Journal of the Acoustical Society of America*, **107 (1)**, 201–220, https://doi.org/10.1121/1.428563.

Henyey, F. S., J. Wright, and S. M. Flatté, 1986: Energy and action flow through the internal wave field: An eikonal approach. *J. Geophys. Res.*, **91 (C7)**, 8487–8495.

Hiron, L., and Coauthors, 2025: The influence of vertical resolution on internal tide energetics and subsequent effects on underwater acoustic propagation. *Journal of Advances in Modeling Earth Systems*, **17 (1)**, e2024MS004 389, https://doi.org/https://doi.org/10.1029/2024MS004389.

Huang, Y., A. Bracco, J. Gula, and K. Polzin, 2025, submitted: Submesoscale circulations, tidal forcing, energy transfers and mixing in model simulations of the deep brazil basin. *Journal of Physical Oceanography*.

Ilicak, M., A. J. Adcroft, S. M. Griffies, and R. W. Hallberg, 2012: Spurious dianeutral mixing and the role of momentum closure. *om*, **45-46**, 37–58.

Kelly, S. M., N. L. Jones, J. D. Nash, and A. F. Waterhouse, 2013: The geography of semidiurnal mode-1 internal-tide energy loss. *Geophysical Research Letters*, **40**, https://doi.org/10.1002/grl.50872.

Kumar, N., and Coauthors, 2021: The inner-shelf dynamics experiment. *Bulletin of the American Meteorological Society*, **102 (5)**, E1033 – E1063, https://doi.org/10.1175/BAMS-D-19-0281.1.

Kunze, E., E. Firing, J. Hummon, T. K. Chereskin, and A. M. Thurnherr, 2006: Global abyssal mixing inferred from lowered ADCP shear and CTD strain profiles. *J. Phys. Oceanogr.*, **36 (8)**, 1553–1576.

Lien, R.-C., T. B. Sanford, J. A. Carlson, and J. H. Dunlap, 2016: Autonomous microstructure EM-APEX floats. *Methods in Oceanography*, **17**, 282–295.

Little, A. D., 1966: Internal waves: Their influence upon naval operations. Tech. Rep. Project Serial Number Sf-101-03-21, Department Of The Navy Bureau Of Ships, Cambridge, Massachusetts. URL https://apps.dtic.mil/sti/tr/pdf/AD0632010.pdf.

Liu, S., Z. Xu, J. You, P. Zhang, X. Li, and Z. Cai, 2025: Deep learning forecast of semidiurnal internal tides from the mariana arc. *Journal of Geophysical Research: Machine Learning and Computation*, **2 (1)**, e2024JH000 363, https://doi.org/https://doi.org/10.1029/2024JH000363.

Lucas, A., P. Franks, and C. Dupont, 2011: Horizontal internal-tide fluxes support elevated phytoplankton productivity over the inner continental shelf. *Limnology & Oceanography: Fluids & Environments*, **1**, 56–74.

Lucas, A. J., and R. Pinkel, 2022: Observations of coherent transverse wakes in shoaling nonlinear internal waves. *Journal of Physical Oceanography*, **52 (6)**, 1277 – 1293, https://doi.org/10.1175/JPO-D-21-0059.1, URL https://journals.ametsoc.org/view/journals/phoc/52/6/JPO-D-21-0059.1.xml.

Luecke, C. A., and Coauthors, 2017: The global mesoscale eddy available potential energy field in models and observations. *Journal of Geophysical Research Oceans*, **122**, 9126–9143, https://doi.org/10.1002/2017JC013136.

Lynch, J. F., Y.-T. Lin, T. F. Duda, and A. E. Newhall, 2010: Acoustic ducting, reflection, refraction, and dispersion by curved nonlinear internal waves in shallow water. *IEEE Journal of Oceanic Engineering*, **35 (1)**, 12–27, https://doi.org/10.1109/JOE.2009.2038512.

MacKinnon, J. A., and Coauthors, 2017: Climate process team on internal-wave driven ocean mixing. *Bulletin of the American Meteorological Society*, **98 (11)**, 2429–2454, https://doi.org/10.1175/BAMS-D-16-0030.1.

Martin, M. J., I. Hoteit, L. Bertino, and A. M. Moore, 2025: Data assimilation schemes for ocean forecasting: state of the art. *State of the Planet*, **5-opsr**, 9, https://doi.org/10.5194/sp-5-opsr-9-2025, URL https://sp.copernicus.org/articles/5-opsr/9/2025/.

Martin, S. A., G. E. Manucharyan, and P. Klein, 2024: Deep learning improves global satellite observations of ocean eddy dynamics. *Geophysical Research Letters*, **51 (17)**, e2024GL110 059, https://doi.org/https://doi.org/10.1029/2024GL110059.

Mazloff, M. R., B. Cornuelle, S. T. Gille, and J. Wang, 2020: The importance of remote forcing for regional modeling of internal waves. *Journal of Geophysical Research: Oceans*, **125 (2)**, e2019JC015 623, https://doi.org/https://doi.org/10.1029/2019JC015623.

Melet, A., S. Legg, and R. Hallberg, 2016: Climatic impacts of parameterized local and remote tidal mixing. *Journal of Climate*, **29 (10)**, 3473–3500.

Miller, U. K., C. J. Zappa, S. F. Zippel, J. T. Farrar, and R. A. Weller, 2023: Scaling of moored surface ocean turbulence measurements in the southeast pacific ocean. *Journal of Geophysical Research: Oceans*, **128 (1)**, e2022JC018 901, https://doi.org/https://doi.org/10.1029/2022JC018901, URL https://agupubs.onlinelibrary.wiley.com/doi/abs/

730 10.1029/2022JC018901, e2022JC018901 2022JC018901, https://agupubs.onlinelibrary.wiley.
731 com/doi/pdf/10.1029/2022JC018901.

732 Moum, J. N., and Coauthors, 2023: Flippin' χsolo, an upper-ocean autonomous turbulence-
733 profiling float. *Journal of Atmospheric and Oceanic Technology*, **40 (5)**, 629 – 644,
734 https://doi.org/10.1175/JTECH-D-22-0067.1, URL https://journals.ametsoc.org/view/journals/
735 atot/40/5/JTECH-D-22-0067.1.xml.

736 Müller, P., G. Holloway, F. Henyey, and N. Pomphrey, 1986: Nonlinear interactions among internal
737 gravity waves. *Reviews of Geophysics*, **24**, 483–536, https://doi.org/10.1029/RG024i003p00493.

738 Munk, W., and C. Wunsch, 1998a: Abyssal Recipes II: energetics of tidal and wind mixing.
739 *Deep-Sea Research I*, **45**, 1977–2010, https://doi.org/10.1016/S0967-0637(98)00070-3.

740 Munk, W. H., 1981: Internal waves and small-scale processes. *Evolution of Physical Oceanogra-*
741 *phy*, B. A. Warren, and C. Wunsch, Eds., MIT Press, 264–281.

742 Munk, W. H., and C. Wunsch, 1998b: Energetics of tidal and wind mixing: abyssal recipes.
743 *Deep-Sea Research I*, **45 (12)**, 1.

744 Nansen, F., 1897: *Farthest North: The epic adventure of a visionary explorer*. Skyhorse Publishing.

745 Nelson, A. D., B. K. Arbic, D. Menemenlis, W. R. Peltier, M. H. Alford, N. Grisouard, and
746 J. M. Klymak, 2020: Improved internal wave spectral continuum in a regional ocean model.
747 *Journal of Geophysical Research: Oceans*, **125 (5)**, e2019JC015 974, https://doi.org/10.1029/
748 2019JC015974.

749 Neuman, S., 2021: What is an 'internal wave'? It might explain the loss of an Indonesian
750 submarine. *National Public Radio*, https://doi.org/https://www.npr.org/2021/04/30/992496772/
751 what-is-an-internal-wave-it-might-explain-the-loss-of-an-indonesian-submarine, date pub-
752 lished: 2021-4-30.

753 Ngodock, H. E., and M. J. Carrier, 2014: A 4d-var assimilation system for the navy coastal
754 ocean model part ii: strong and weak constraints assimilation experiments with real ob-
755 servations in the monterey bay. *Monthly Weather Review*, **142**, 2108–2117, https://doi.org/
756 10.1175/MWR-D-13-00220.1.

Ngodock, H. E., I. Souopgui, A. J. Wallcraft, J. G. Richman, J. F. Shriver, and B. K. Arbic, 2016: On improving the accuracy of the m_2 barotropic tides embedded in a high-resolution global ocean circulation model. *Ocean Modelling*, **97**, 16–26, https://doi.org/10.1016/j.ocemod.2015.10.011.

Niwa, Y., and T. Hibiya, 2001: Numerical study of the spatial distribution of the m2 internal tide in the pacific ocean. *Journal of Geophysical Research: Oceans*, **106 (C10)**, 22 441–22 449, https://doi.org/https://doi.org/10.1029/2000JC000770.

NOAA, 2023: Global surge and tide operational forecast system 2-d (stofs-2d-global), accessed on 2023-02-03.

Pelaez Quiñones, J. D., and Coauthors, 2023: High resolution seafloor thermometry for internal wave and upwelling monitoring using distributed acoustic sensing. *Scientific Reports*, **13 (1)**, 17 459.

Pinkel, R., M. A. Goldin, J. A. Smith, O. M. Sun, A. A. Aja, M. N. Bui, and T. Hughen, 2011: The wirewalker: A vertically profiling instrument carrier powered by ocean waves. *Journal of Atmospheric and Oceanic Technology*, **28 (3)**, 426–435, https://doi.org/10.1175/2010JTECHO805.1, URL https://journals.ametsoc.org/view/journals/atot/28/3/2010jtecho805_1.xml.

Polzin, K. L., 2025: Covariance based estimates of near-boundary diapycnal upwelling in a submarine canyon. *J. Physical Oceanogr.*, **in prep.**

Polzin, K. L., and Y. V. Lvov, 2011: Toward regional characterizations of the oceanic internal wavefield. *Reviews of geophysics*, **49 (4)**.

Polzin, K. L., and T. J. McDougall, 2022: Mixing at the ocean's bottom boundary. *Ocean Mixing*, Elsevier, 145–180.

Polzin, K. L., J. M. Toole, J. R. Ledwell, and R. W. Schmitt, 1997: Spatial variability of turbulent mixing in the abyssal ocean. *Science*, **276**, 93–96, https://doi.org/10.1126/science.276.5309.93.

Polzin, K. L., J. M. Toole, and R. W. Schmitt, 1995: Finescale parameterization of turbulent dissipation. *Journal of Physical Oceanography*, **25**, 306–328, https://doi.org/10.1175/1520-0485(1995)025⟨0306:FPOTD⟩2.0.CO;2.

Polzin, K. L., B. Wang, Z. Wang, F. Thwaites, and A. J. Williams, 2021: Moored flux and dissipation estimates from the northern deepwater gulf of mexico. *Fluids*, **6 (7)**, 237.

Qiu, B., S. Chen, J. Wang, and L.-L. Fu, 2024: Seasonal and fortnight variations in internal solitary waves in the indonesian seas from the swot measurements. *Journal of Geophysical Research: Oceans*, **129 (7)**, e2024JC021 086, https://doi.org/https://doi.org/10.1029/2024JC021086.

Raja, K. J., M. C. Buijsman, A. Bozec, R. W. Helber, J. F. Shriver, A. Wallcraft, E. P. Chassignet, and B. K. Arbic, 2024: Spurious internal wave generation during data assimilation in eddy resolving ocean model simulations. *Ocean Modelling*, **188**, 102 340, https://doi.org/https://doi.org/10.1016/j.ocemod.2024.102340.

Raja, K. J., M. C. Buijsman, J. F. Shriver, B. K. Arbic, and O. Siyanbola, 2022: Near-inertial wave energetics modulated by background flows in a global model simulation. *Journal of Physical Oceanography*, **52 (5)**, 823–840, https://doi.org/10.1175/JPO-D-21-0130.1.

Ramadhan, A., and Coauthors, 2020: Oceananigans.jl: Fast and friendly geophysical fluid dynamics on GPUs. *Journal of Open Source Software*, **5 (53)**, 2018, https://doi.org/10.21105/joss.02018, URL https://doi.org/10.21105/joss.02018.

Ray, R. D., and G. T. Mitchum, 1996: Surface manifestation of internal tides generated near hawaii. *Geophysical Research Letters*, **23 (16)**, 2101–2104.

Rocha, C. B., T. K. Chereskin, S. T. Gille, and D. Menemenlis, 2016: Mesoscale to submesoscale wavenumber spectra in Drake Passage. *Journal of Physical Oceanography*, **46**, 601–620, https://doi.org/10.1175/JPO-D-15-0087.1.

Rumelhart, D. E., G. E. Hinton, and R. J. Williams, 1986: Learning representations by back-propagating errors. *Nature*, **323 (6088)**, 533–536.

Sanford, T. B., 1971: Motionally induced electric and magnetic fields in the sea. **76**, 3467–3492.

Sanford, T. B., J. H. Dunlap, J. A. Carlson, D. C. Webb, and J. B. Girton, 2005: Autonomous velocity and density profiler: EM-APEX. *Proceedings of the IEEE/OES Eighth Working Conference on Current Measurement Technology*, 152–156.

Santos-Ferreira, A. M., and Coauthors, 2025: The internal waves service workshop: Observing internal waves globally with deep learning and synthetic aperture radar. *Bulletin of the American Meteorological Society*, https://doi.org/10.1175/BAMS-D-25-0133.1.

Shchepetkin, A. F., and J. C. McWilliams, 2005: The Regional Oceanic Modeling System: A split-explicit, free-surface, topography-following-coordinate oceanic model. *Ocean Modelling*, **9**, 347–404.

Simmons, H. L., and M. H. Alford, 2012: Simulating the long-range swell of internal waves generated by ocean storms. *Oceanography*, **25**, 30–41, URL https://doi.org/10.5670/oceanog.2012.39.

Simmons, H. L., R. W. Hallberg, and B. K. Arbic, 2004: Internal wave generation in a global baroclinic tide model. *Deep-Sea Research II*, **51**, 3043–3068.

Sinnett, G., K. A. Davis, A. J. Lucas, S. N. Giddings, E. Reid, M. E. Harvey, and I. Stokes, 2020: Distributed temperature sensing for oceanographic applications. *Journal of Atmospheric and Oceanic Technology*, **37 (11)**, 1987 – 1997, https://doi.org/10.1175/JTECH-D-20-0066.1.

Siyanbola, O. Q., M. C. Buijsman, A. Delpech, R. Barkan, Y. Pan, and B. K. Arbic, 2024: Interactions of remotely generated internal tides with the u.s. west coast continental margin. *Journal of Geophysical Research: Oceans*, **129 (6)**, e2023JC020 859, https://doi.org/https://doi.org/10.1029/2023JC020859.

Siyanbola, O. Q., M. C. Buijsman, A. Delpech, L. Renault, R. Barkan, J. F. Shriver, B. K. Arbic, and J. C. McWilliams, 2023: Remote internal wave forcing of regional ocean simulations near the u.s. west coast. *Ocean Modelling*, **181**, 102 154, https://doi.org/10.1016/j.ocemod.2022.102154.

Skitka, J., B. K. Arbic, Y. Ma, K. Momeni, Y. Pan, W. R. Peltier, D. Menemenlis, and R. Thakur, 2024a: Internal-wave dissipation mechanisms and vertical structure in a high-resolution regional ocean model. *Geophysical Research Letters*, **51 (17)**, e2023GL108 039, https://doi.org/https://doi.org/10.1029/2023GL108039.

Skitka, J., B. K. Arbic, R. Thakur, D. Menemenlis, W. R. Peltier, Y. Pan, K. Momeni, and Y. Ma, 2024b: Probing the nonlinear interactions of supertidal internal waves using a high-resolution

regional ocean model. *Journal of Physical Oceanography*, **54 (2)**, 399–425, https://doi.org/https://10.1175/JPO-D-22-0236.1.

Spence, D., O. Kitzler, C. Taylor, S. Curtis, B. Neimann, J. Dawes, J. Downes, and H. Pask, 2024: Depth-resolved water temperature measurements using raman lidar. *Applied Optics*, **63 (16)**, 4366–4371.

Srinivasan, A., T. M. Chin, E. P. Chassignet, M. Iskandarani, and N. Groves, 2022: A statistical interpolation code for ocean analysis and forecasting. *Journal of Atmospheric and Oceanic Technology*, **39 (3)**, 367–386, https://doi.org/10.1175/JTECH-D-21-0033.1.

Sun, B., Z. Jing, M. Yuan, H. Yang, and L. Wu, 2024: Effects of horizontal resolution on long-range equatorward radiation of near-inertial internal waves in ocean general circulation models. *Journal of Advances in Modeling Earth Systems*, **16 (9)**, e2024MS004 216, https://doi.org/https://doi.org/10.1029/2024MS004216.

Sun, S., R. Bleck, C. G. Rooth, J. Dukowicz, E. P. Chassignet, and P. Killworth, 1999: Inclusion of thermobaricity in isopycnic-coordinate ocean models. *Journal of Physical Oceanography*, **29**, 2719–2729.

SWOT, 2024a: Swot level 2 karin low rate sea surface height data product version c. NASA Physical Oceanography Distributed Active Archive Center, CA, USA. Accessed 2025-06-01, https://doi.org/10.5067/SWOT-SSH-2.0.

SWOT, 2024b: Swot postlaunch oceanography field campaign l2 moorings ver. 1. NASA Physical Oceanography Distributed Active Archive Center, CA, USA. Accessed 2025-02-01, https://doi.org/10.5067/SWTPO-MOOR2.

Tchonang, B., and coauthors, 2025: SWOT Geostrophic Velocity Validation against in-situ measurements in the California Current. *Earth and Space Science*, **in prep**.

Varma, D., M. Buijsman, O. Q. Siyanbola, M. Andres, and A. F. Waterhouse, 2025: A multivariable plane-wave fit technique to extract unidirectional internal wave fluxes from an internal wave resolving mooring array. *Journal of Atmospheric and Oceanic Technology*, **in preparation**.

Villamaña, M., and Coauthors, 2017: Role of internal waves on mixing, nutrient supply and phytoplankton community structure during spring and neap tides in the upwelling ecosystem of Ria de Vigo (NW Iberian Peninsula). *Limnology and Oceanography*, **15**, 1014–1030.

Wagner, G. L., and Coauthors, 2025: High-level, high-resolution ocean modeling at all scales with Oceananigans. *arXiv preprint*, https://doi.org/10.48550/arXiv.2502.14148, 2502.14148.

Wang, J., and Coauthors, 2022: On the development of SWOT in-situ Calibration/Validation for short-wavelength ocean topography. *Journal of Atmospheric and Oceanic Technology*, https://doi.org/10.1175/JTECH-D-21-0039.1, place: Boston MA, USA Publisher: American Meteorological Society.

Wang, J., and Coauthors, 2025: Swot mission validation of sea surface height measurements at sub-100 km scales. *Geophysical Research Letters*, https://doi.org/10.1029/2025GL114936.

Waterhouse, A. F., and Coauthors, 2014: Global patterns of diapycnal mixing from measurements of the turbulent dissipation rate. *Journal of Physical Oceanography*, **44**, 1854–1872, https://doi.org/10.1175/JPO-D-13-0104.1.

Weaver, A., 2003: 3d-var and 4d-var approaches to ocean data assimilation. Ph.D. thesis, 57-66 pp., Shinfield Park, Reading.

Whalen, C. B., J. A. MacKinnon, L. D. Talley, and A. F. Waterhouse, 2015: Estimating the mean diapycnal mixing using a finescale strain parameterization. *Journal of Physical Oceanography*, **45**, 1174–1188, https://doi.org/10.1175/JPO-D-14-0167.1.

White, L., and A. J. Adcroft, 2008: A high-order finite volume remapping scheme for nonuniform grids: The piecewise quartic method (PQM). *J. Comp. Phys.*, 7394–7422.

White, L., A. J. Adcroft, and R. W. Hallberg, 2009: High-order regridding-remapping schemes for continuous isopycnal and generalized coordinates in ocean models. *J. Comp. Phys.*, **228**, 8665–8692.

Whitley, V., and J. Wenegrat, 2025: Breaking internal waves on sloping topography: connecting parcel displacements to overturn size, interior-boundary exchanges, and mixing. *Journal of Physical Oceanography*, https://doi.org/10.1175/JPO-D-24-0052.1.

Whitwell, C. A., N. L. Jones, G. N. Ivey, M. G. Rosevear, and M. D. Rayson, 2024: Ocean mixing in a shelf sea driven by energetic internal waves. *Journal of Geophysical Research: Oceans*, **129 (2)**, e2023JC019 704, https://doi.org/https://doi.org/10.1029/2023JC019704, URL https://agupubs.onlinelibrary.wiley.com/doi/abs/10.1029/2023JC019704, e2023JC019704 2023JC019704, https://agupubs.onlinelibrary.wiley.com/doi/pdf/10.1029/2023JC019704.

Wunsch, C., and R. Ferrari, 2004: Vertical mixing, energy and the general circulation of the oceans. *Annual Review of Fluid Mechanics*, **36 (1)**, 281–314, https://doi.org/10.1146/annurev.fluid.36.050802.122121.

Xu, C., and E. D. Zaron, 2024: Detecting instantaneous tidal signals in ocean models utilizing streaming band-pass filters. *james*, **16**, e2024MS004 319.

Xu, C., and E. D. Zaron, 2025: Parameterization of frequency-dependent internal wave drag in global ocean models. *james*, **submitted**.

Xu, X., E. P. Chassignet, A. J. Wallcraft, B. K. Arbic, M. C. Buijsman, and M. Solano, 2022: On the spatial variability of the mesoscale sea surface height wavenumber spectra in the atlantic ocean. *Journal of Geophysical Research: Oceans*, **127 (10)**, e2022JC018 769, https://doi.org/10.1029/2022JC018769.

Yadidya, B., 2023: Replication Data for: "Phase-accurate internal tides in a global ocean forecast model: Potential applications for nadir and wide-swath altimetry". Harvard Dataverse, https://doi.org/10.7910/DVN/HMDTRZ.

Yadidya, B., B. K. Arbic, J. F. Shriver, A. D. Nelson, E. D. Zaron, M. C. Buijsman, and R. Thakur, 2024: Phase-accurate internal tides in a global ocean forecast model: Potential applications for nadir and wide-swath altimetry. *Geophysical Research Letters*, **51 (4)**, e2023GL107 232, https://doi.org/https://doi.org/10.1029/2023GL107232.

Zaron, E. D., 2019a: Baroclinic tidal sea level from exact-repeat mission altimetry. *J. Phys. Oceanogr.*, **49**, 193–210, https://doi.org/10.1175/JPO-D-18-0127.1.

Zaron, E. D., 2019b: Baroclinic tidal sea level from exact-repeat mission altimetry. *jpo*, **49 (1)**, 193–210.

Zaron, E. D., and R. D. Ray, 2023: Clarifying the distinction between steric and baroclinic sea surface height. *jpo*, **53 (11)**, 2591–2596.

Zeiden, K., J. Thomson, A. Shcherbina, and E. D'Asaro, 2024: Observations of elevated mixing and periodic structures within diurnal warm layers. *Journal of Geophysical Research: Oceans*, **129 (11)**, e2024JC021 399, https://doi.org/https://doi.org/10.1029/2024JC021399, URL https://agupubs.onlinelibrary.wiley.com/doi/abs/10.1029/2024JC021399, e2024JC021399 2024JC021399, https://agupubs.onlinelibrary.wiley.com/doi/pdf/10.1029/2024JC021399.

Zhang, X., X. Li, and Q. Zheng, 2021: A machine-learning model for forecasting internal wave propagation in the andaman sea. *IEEE Journal of Selected Topics in Applied Earth Observations and Remote Sensing*, **14**, 3095–3106, https://doi.org/10.1109/JSTARS.2021.3063529.

Zhao, Z., M. Alford, J. Girton, L. Rainville, and H. Simmons, 2016: Global observations of open-ocean mode-1 M_2 internal tides. *Journal of Physical Oceanography*, **46**, 1657–1684.

Zulberti, A., N. L. Jones, and G. N. Ivey, 2020: Observations of enhanced sediment transport by nonlinear internal waves. *Geophys. Res. Lett.*, **47**, e2020GL088 499.